Article:

Canal-Solis, K.V., Tindall, J.C., Oldeman, A.M. et al. (2025) Asymmetric Pacific variability in the Pliocene: An unchanged PDO relative to a suppressed ENSO. Global and Planetary Change, 253. 104932. ISSN: 0921-8181

https://doi.org/10.1016/j.gloplacha.2025.104932

Global and Planetary Change 253 (2025) 104932

Contents lists available at ScienceDirect

Global and Planetary Change

journal homepage: www.elsevier.com/locate/gloplacha

Research Article

Asymmetric Pacific variability in the Pliocene: An unchanged PDO relative to a suppressed ENSO☆

Katya V. Canal-Solis[a,b,*], Julia C. Tindall[a], Arthur M. Oldeman[c], Alan M. Haywood[a], Ayako Abe-Ouchi[d], Michiel L.J. Baatsen[c], Wing-Le Chan[d], Ran Feng[e], Stephen J. Hunter[a], Xiangyu Li[f,g], Christian Stepanek[h], Zhongshi Zhang[f,g]

[a] School of Earth and Environment, University of Leeds, Woodhouse Lane, Leeds, West Yorkshire LS2 9JT, UK
[b] The Lyell Centre, Heriot-Watt University, Edinburgh, UK
[c] Institute for Marine and Atmospheric research Utrecht (IMAU), Department of Physics, Utrecht University, 3584 CC Utrecht, the Netherlands
[d] Atmosphere and Ocean Research Institute, University of Tokyo, Kashiwa, Japan
[e] University of Connecticut, Storrs, 06269, United States of America
[f] Department of Atmospheric Science, School of Environmental Studies, China University of Geosciences, Wuhan, China
[g] Centre for Severe Weather and Climate and Hydro-geological Hazards, Wuhan, China
[h] Alfred Wegener Institute - Helmholtz Centre for Polar and Marine Research, Am Handelshafen 12, Bremerhaven, Germany

ARTICLE INFO

Keywords:
PDO
ENSO
Pacific variability
Climate variability
Pliocene
PlioMIP2

ABSTRACT

Currently, the El Niño Southern Oscillation (ENSO) dominates the climate variability in the Pacific basin, while the Pacific Decadal Oscillation (PDO) is the second dominant mode of variability. Both modes of variability are crucial due to their global roles. However, the response of PDO and ENSO to changes in forcing, such as increased atmospheric CO_2 concentrations or geography, is not fully understood. Past intervals of geological time offer valuable insights to understand their responses to different forcing. Here, we investigate PDO and ENSO behaviour and their relationship in the mid-Pliocene Warm Period (MP; ~3 million years ago) using the Pliocene Model Intercomparison Project version 2 (PlioMIP2) climate model ensemble. Results show that in the MP, although ENSO variability is robustly suppressed, PDO variability remains similar to the pre-industrial (PI) in terms of spatial pattern and multi model mean (MMM) amplitude, although individual models differ. The predominant frequencies of variability in the Pacific basin shift from interannual (3–4 years) in the PI to decadal (15–35 years) in the MP. Relative to a weakened ENSO, PDO is a more important mode of Pacific variability in the MP. The linear relationship between PDO and ENSO decreases by only 18 % in the MP even though ENSO variability decreases by ~30 %, suggesting that the majority of PDO variability is not directly explained by changes in ENSO variability. We suggest that these results are driven by MP boundary conditions other than elevated CO_2 levels.

1. Introduction

The Pacific basin has two dominant modes of climate variability: the El Niño-Southern Oscillation (ENSO) and the Pacific Decadal Oscillation (PDO). Today's leading mode of variability, ENSO, is located in the equatorial Pacific basin and is the main global interannual mode of variability, with typical periods of 2–7 years (McPhaden et al., 2006). The second mode of variability, PDO, is the dominant decadal mode of variability in the North Pacific Ocean (Mantua and Hare, 2002), typically oscillating with a periodicity of 20–30 years. Both ENSO and PDO are formed by atmosphere-ocean interactions which oscillate between two extreme phases: a warm phase (El Niño and the positive PDO phase, respectively) and a cool phase (La Niña and the negative PDO phase, respectively; McPhaden et al., 2006; Mantua et al., 1997; Mantua and Hare, 2002). ENSO has global teleconnections that impact natural systems and human societies, such as increased rates of wildfires in Australia during El Niño (Wang and Hendon, 2007) or increased typhoon activity and intensity (Hsu et al., 2013). Meanwhile, PDO also

☆ This article is part of a Special issue entitled: 'PlioMIP3' published in Global and Planetary Change.

* Corresponding author at: School of Earth and Environment, University of Leeds, Woodhouse Lane, Leeds, West Yorkshire LS2 9JT, UK.
E-mail address: kvc3000@hw.ac.uk (K.V. Canal-Solis).

https://doi.org/10.1016/j.gloplacha.2025.104932
Received 19 November 2024; Received in revised form 27 May 2025; Accepted 9 June 2025
Available online 12 June 2025

has far-reaching links: it is connected to ENSO, where the general view is that ENSO variability leads PDO variability through oceanic Rossby waves (Newman et al., 2016; Nidheesh et al., 2017). Furthermore, the variability of PDO is related to the atmospheric variations in the North Pacific, namely the variability of the Aleutian low (AL) pressure system, which is thought to lead PDO variability through surface wind forcing (Di Lorenzo et al., 2013; Newman et al., 2016). PDO teleconnections can lead to precipitation changes or multi decadal droughts in North and South America, Asia, and Australia (Hare and Mantua, 2000). In addition, the role of the PDO in oceanic energy redistribution is thought to be important (Trenberth and Fasullo, 2013; Yan et al., 2016).

Although understanding the behaviour of ENSO and PDO is crucial to comprehend the Earth's climate system overall, there are still gaps of knowledge on their behaviour and responses to different perturbations. It is essential to develop studies that aid the understanding of ENSO and PDO behaviour to different perturbations because of the worldwide impact of these two modes of climate variability. In the context of climate change, it is especially important to understand the responses of ENSO and PDO to changes in different atmospheric CO_2 concentrations that result in a modification of radiative forcing on Earth's climate. In addition, studying ENSO and PDO dynamics at longer time scales than the current observational period is important towards capturing a more complete picture of their range of variability.

Much research has addressed ENSO and PDO behaviour at different atmospheric CO_2 concentrations with a focus on the future. Studies of ENSO variability in climate change scenarios show disagreement, implying that the ENSO responses remain not fully comprehended. For instance, using the Representative Concentration Pathway 8.5 (RCP8.5), Cai et al. (2014) found an increased frequency but no substantial change in the amplitude of the eastern Pacific ENSO towards 2090. Conversely, using the same RCP8.5, Kim et al. (2014) showed that ENSO response to global warming is not linear in time, and ENSO amplitude is projected to increase until ~2040 but to decrease thereafter. Geng et al. (2023) found that, relative to the historical period, La Niña events occurred more frequently at a range from 13 to 33 % towards 2099 under a range of low to high Shared Socioeconomical Pathways (SSPs). PDO changes are also uncertain. As such, Liguori and Lorenzo (2018) suggested that the Pacific Decadal Variability might be amplified towards 2100 in the RCP8.5 high-emission scenario due to the intensification of the North Pacific Meridional Mode through the winds-evaporation-SST feedback caused by the anthropic warming effect. Conversely, it is expected to significantly decrease its amplitude and increase its frequency in different CO_2 emission scenarios, possibly related to Rossby waves speeding up, leaving less time for a complete PDO development (Geng et al., 2019; S. Li et al., 2020). According to the IPCC AR6, this PDO change towards decreased amplitude and higher frequency is considered to have medium confidence under the effect of current levels of global warming and low confidence for future changes (Lee et al., 2023). The level of uncertainty emphasizes the need for more detailed investigation to better understand PDO variability and mechanisms.

The relationship between ENSO and PDO has been mostly studied with an emphasis on the recent historical and future periods. Studies for the recent historical period, such as Verdon and Franks (2006), found that similar phases (cold or warm) of PDO and ENSO tend to coincide. Hence, when the El Niño is present, a PDO warm phase tends to take place at an increased frequency and vice versa for PDO cold phases and La Niña events (Verdon and Franks, 2006). For future climate change scenarios, the linear relationship between ENSO and PDO could be stronger (Kwon et al., 2013), which means that the ENSO influence over PDO is expected to become stronger than in the present. In addition, the response of PDO to ENSO mainly depends on the amplitude of ENSO (i.e., a higher ENSO amplitude leads to a stronger correlation with PDO) and on the strength of the ENSO–AL teleconnection, which in turn depends on specific features of global climate models (Nidheesh et al., 2017).

To gain a more complete understanding of the climate variability and change, we should extend our research on PDO and ENSO variability beyond the modern and near future period. Past intervals of geological time could help us better understand the response of modes of climate variability to perturbation, including increased atmospheric CO_2 concentrations. Specifically, the mid-Pliocene Warm Period (MP) is a geological interval with a continental configuration that is quite similar to that of today compared to earlier past warm periods. The MP is characterised by a mean global temperature between 1.7 and 5.2 °C above the pre-industrial (PI) temperature, with best estimates of atmospheric CO_2 levels around 400 ppm (Haywood et al., 2020). While the distribution of land versus sea including topography and bathymetry was similar to the present, ice sheets were reduced compared to the PI (Dowsett et al., 2016). These features make the MP an interesting period to study the climate system in a quasi-equilibrium state of increased CO_2 atmospheric concentrations. Furthermore, it is suggested that the MP is considered an analogue to the possible climate at the end of the 21st century in terms of temperature and precipitation considering medium emission scenarios, similar to the RCP4.5 (Burke et al., 2018) or SSP2-4.5 and SSP3-7.0 scenarios depending on the variable, spatial domain and temporal aggregation (Burton et al., 2024).

The Pliocene Model Intercomparison Project (PlioMIP) uses model ensembles to study the MP in detail (Haywood et al., 2010). PlioMIP has completed two phases of work: PlioMIP1 and 2 (Haywood et al., 2010; Haywood et al., 2016), with the third phase currently underway (Haywood et al., 2024). PlioMIP2 is focussed on the MIS KM5c interglacial time slice (~3.205 Ma), which has orbital forcing parameters very similar to the present. In addition, it uses the PRISM4 (Pliocene Research, Interpretation and Synoptic Mapping version 4; Dowsett et al., 2016) palaeoenvironmental reconstruction as standardised boundary conditions (Haywood et al., 2016). PRISM4 includes a sea-land mask with presence of an above-sea Central American Seaway, closing of Bering Strait and Canadian Arctic Archipelago and inclusion of independent bathymetry and elevation (Dowsett et al., 2016).

Various studies analysing proxy data have contributed to gaining an understanding of ENSO during the MP, however, significant uncertainty remains in terms of ENSO behaviour. For example, some studies suggest a small zonal sea surface temperature (SST) gradient in the tropical Pacific (a 'permanent El Niño-like' mean state) or even no ENSO variability (e.g., Molnar and Cane, 2002; Wara et al., 2005; Fedorov et al., 2006; Ravelo et al., 2006; Seki et al., 2012). On the other hand, Watanabe et al. (2011) reconstructed marked ENSO variability, similar to Scroxton et al. (2011). More recently, White and Ravelo (2020) used proxy data corresponding to the early Pliocene and found a reduced ENSO amplitude. Initial modelling efforts confirmed the existence of an interannual variability of ENSO with a deep thermocline in the tropical Pacific (Scroxton et al., 2011). In addition, marked ENSO variability was shown, no matter the equatorial Pacific mean state using fully coupled climate model experiments (e.g., Bonham et al., 2009; Haywood et al., 2007; von der Heydt et al., 2011).

Studies using fully coupled models from the PlioMIP1 project (phase one of PlioMIP) investigated ENSO, PDO and their linkages. Using the NorESM-L model, Zhang et al. (2012) detected a weak ENSO in the MP. Furthermore, Brierley (2015) obtained a reduced ENSO amplitude in 8 out of 9 models. Meanwhile, using the HadCM3 model, Tindall et al. (2016) found overall increased ENSO amplitudes but with a strong centennial scale variability of ENSO. Regarding the frequency, Brierley (2015) found that the power spectrum peaks at 5–7 years in the MP versus 3–4 years in the PI. Similarly, Tindall et al. (2016) observed that the MP ENSO in HadCM3 was characterized by longer periodicity than for the PI by ~12 %. In addition, no prevalent ENSO type or flavour was consistently found among the MP model ensemble (Brierley, 2015). For HadCM3 only, however, the prevalent ENSO type tends to be located in the central Pacific (Tindall et al., 2016). The relationship between ENSO and PDO in the MP was also explored using PlioMIP1 models. Specifically, Brierley (2015) found no consistency in PDO amplitude or frequency changes. Meanwhile, Tindall et al. (2016) found a stronger PDO amplitude, as well as a stronger ENSO and PDO relationship using the PlioMIP1 HadCM3 model at a multi centennial scale.

More recently, the PlioMIP2 model ensemble has been employed to study ENSO and AL variability. The MP ENSO simulated in PlioMIP2 shows a consistent interannual variability with reduced amplitudes by ~24 % compared to the PI (Oldeman et al., 2021; Pontes et al., 2022). No clear changes in the dominant frequency were found (Oldeman et al., 2021). The mechanisms associated with the reduced ENSO amplitude were explored by Pontes et al. (2022), who found that a higher relative warmth in the Northern Hemisphere than in the Southern Hemisphere may have played a key role. This asymmetrical temperature anomaly induces an intensification of the subtropical South Pacific Anticyclone, which in turn shifts the Intertropical Convergence Zone (ITCZ) northward, suppressing processes that allow the El Niño or La Niña development. Most recently, Oldeman et al. (2024) showed that atmospheric variability in the North Pacific (i.e. the AL variability) in PlioMIP2 is similar to the PI even with ENSO variability being suppressed. They show that the ENSO–AL teleconnection is similar but find that the main contribution to the AL variability, internal stochastic variability in the atmosphere, is largely unchanged. Even though all these studies are related to ENSO, the North Pacific atmosphere and their link, an investigation of PDO and the ENSO-PDO link using the PlioMIP2 ensemble has not been conducted. In this paper we attempt to fill this gap.

In the present study, our main research question is: How does the behaviour of ENSO and PDO change in the MP according to the PlioMIP2 ensemble? We answer this question by addressing these three specific questions: 1) Do the spatial and temporal properties of ENSO and PDO differ in the MP from the PI? 2) Is ENSO or PDO the dominant mode of variability of the Pacific Ocean in the MP? 3) How does the interaction between ENSO and PDO differ in the MP with respect to PI? To answer these questions, we will analyse datasets that are longer than the typically employed in similar single model and multi-model ensemble studies. These very long datasets allow us to address centennial variability to robustly study the frequency and spatial patterns of SSTs in the Pacific basin in the PlioMIP2 simulations, determine the correlation between ENSO and PDO and identify the multi model differences between ENSO and PDO variability by examining each model.

Our manuscript is structured as follows: Section 2 contains a description of the considered PlioMIP2 models and of the methods that we follow to examine PDO and ENSO. The general perspective is to perform a multi model analysis while considering that, although all models belong to the PlioMIP2, each one of them has particularities that may carry importance for the interpretation of their simulated climate states. Towards gaining an impression of the agreement between models and reconstructions, in Section 3 we first analyse the PI PlioMIP2 models against observational data of recent climate (Section 3.1). After that, we investigate the dominant modes of variability in the Pacific basin (Sections 3.2 and 3.3) and calculate the correlations between the two modes of variability to analyse their relationship (Section 3.4). Finally, we discuss our results (Section 4) and summarise and conclude with final remarks and implications (Section 5).

2. Data and methods

2.1. The PlioMIP2 models

In PlioMIP2, all modelling groups followed the modelling protocols described in Haywood et al. (2016). Further details of simulations provided by any single model can be found in the references provided in Table 1. The PlioMIP2 modelling groups performed at least two main simulations: the mid-Pliocene (named as Eoi^{400}, here referred to as MP) and the pre-industrial control run (named as E^{280}, here referred to as PI). The orbital configuration (eccentricity, obliquity, and precession) for MP and PI was set to the conditions of the PI (1850 CE). This configuration was set so that modelling results from the MP can be easily employed in the context of using paleoclimate to interpret potential future environmental conditions given that the KM5c interglacial time slice used for MP has a very similar orbital forcing to near-modern (Haywood et al., 2016). For models taking part in the fourth iteration of the Paleoclimate Model Intercomparison Project (PMIP4), orbital forcing settings, and the full definition of the PI setup, are described by Otto-Bliesner et al. (2017b). MP and PI simulations were run with CO_2 atmospheric concentrations of 400 ppmv and 280 ppmv, respectively (Haywood et al., 2016) or with the respective settings defined by Otto-Bliesner et al. (2017b) for PMIP4 models. Other greenhouse gases and atmospheric aerosols for MP remain the same as for PI but these might vary between groups. Vegetation has two options to use: static prescribed or dynamic. Only COSMOS used dynamic vegetation (Stepanek et al., 2020), while the rest of the groups used reconstructed vegetation from the Pliocene Research, Interpretation and Synoptic Mapping version 3 (PRISM3; Salzmann et al., 2008), also used in PlioMIP1.

The PlioMIP2 MP paleogeography used in models in this study is overall similar to modern but with important changes that influence atmosphere and ocean circulation. These changes include the closure of the Bering Strait, Hudson Bay and Canadian Archipelago, as well as the presence of the subaerial Sunda and Sahul shelves in Oceania and a closed Central American Seaway (Dowsett et al., 2016; Haywood et al., 2016). The Bering Strait closure might result in a warmer North Atlantic but a cooler North Pacific (Hu et al., 2015), a mechanism related to the intensification of Atlantic Meridional Overturning Circulation (AMOC; Otto-Bliesner et al., 2017a; Weiffenbach et al., 2023). Meanwhile, the presence of Sunda and Sahul shelves created effects on ocean and atmospheric circulation. In specific, the MP Indonesian throughflow is enhanced in 10 out of 15 PlioMIP2 models and the trade winds amplify their intensity over the western Pacific Ocean (Ren et al., 2023). ENSO and PDO may play a role in modulating Indonesian throughflow changes (Wang, 2019). In addition, at high latitudes, energy balance and circulation are influenced by prescribing ice sheet extent that is dramatically decreased with respect to modern conditions in Greenland and the Antarctic (Dowsett et al., 2016; Haywood et al., 2020).

In this study, we use the MP and PI simulations from 7 (Table 1) of

Table 1
PlioMIP2 models used in this paper with indication of the number of years computed in simulations, years analysed by us (last model years of each model simulation) and spatial resolution of the ocean grid.

Model	Total years of MP simulation	Total years of PI simulation	Number of years analysed of MP	Number of years analysed of PI	Spatial resolution	Reference
CCSM4-Utr	2000	3100	~200	200	1.25° × 0.9°	(Baatsen et al., 2022)
CESM1.2	1200	806	599	306	~1° × ~1°	(Feng et al., 2020)
COSMOS	1950	1950	500	500	3.0° × 1.8°	(Stepanek et al., 2020)
HadCM3	2500	2500	500	500	1.25° × 1.25°	(Hunter et al., 2019)
IPSLCM6A-LR	1100	1450	200	200	1.0° × 1.0°	(Lurton et al., 2020)
MIROC4m	4000	2220	500	500	1.4° × 1.4°	(Chan and Abe-Ouchi, 2020)
NorESM-L	2200	1200	198	200	~3° × ~3°	(X. Li et al., 2020)

the total ensemble of 17 PlioMIP2 models. The PI and MP simulations were both run for at least 500 years (longer in most models) so that the simulations are in a quasi-equilibrium state with the boundary conditions. In this study, we use models that have supplied at least close to 200 years of monthly SSTs model output after spin-up for analysis, as shorter periods may be insufficient to fully investigate multi decadal oscillations. The length of the model output time series employed by us is beyond the typical analysis period in model intercomparisons. Consequently, we used only 7 models from the whole PlioMIP2 ensemble, most of them obtained by direct request to the modelling group leaders. The only exception was for IPSLCM6A-LR data, which was downloaded in full from the CMIP6 repository (ESGF). The datasets described in Table 1 were regridded to a common resolution of 1°x1° using linear interpolation to aid the comparison between models and to analyse the multi model mean (MMM). After that, the SST anomalies were calculated by removing the mean annual cycle from each grid cell.

2.2. Model evaluation

PI SSTs were evaluated using the reconstructed gridded product NOAA Extended Reconstructed Sea Surface Temperature (ERSST) version 5 (NOAA ERSSTv5). The NOAA ERSSTv5 is a historical reconstruct observational product containing different input datasets of ocean surface and near-surface observations and sea ice concentration that were interpolated and bias-adjusted with realistic spatiotemporal variations for 1854–present (Huang et al., 2017). Here, we use the monthly NOAA ERSSTv5 for 149 years (1870–2018). As the reconstructed observational 1870–2018 period is not exactly the pre-industrial period and includes the anthropogenic warming effect, we detrended this dataset using a linear regression method.

The evaluation aims at analysing the variance of the SST anomalies of the PI simulation with respect to reconstructed observational data. To verify that SST variability in the PI simulation is realistic for our domain of interest, we compared the variance of the SST anomalies of NOAA ERSSTv5 and the PI simulations in three regions: tropical Pacific (150° E–80° W; 20° S–20° N), North Pacific (120° E–120° W; 20° N–70° N) and the Pacific basin (120° E–70° W; 60° S–70° N). We also computed the relative change in variance in the MP relative to the PI.

Although it would be desirable to also verify the variability in the MP simulations against model independent sources of information, proxy data from the Pliocene is insufficient for analysing temporal variability or spatial SST patterns related to ENSO or the PDO. Nevertheless, the MP mean state of PlioMIP2 simulations has been previously evaluated by comparison against mean temperatures from proxies (Foley and Dowsett, 2019; Haywood et al., 2020; McClymont et al., 2020; Tindall et al., 2022), including from 5 sites in the equatorial Pacific and 4 in the North Pacific. Oldeman et al. (2021) also performed a model–proxy comparison of SSTs at 6 sites in the tropical Pacific based on reconstructions by (Foley and Dowsett, 2019; McClymont et al., 2020) and found a reasonable general agreement. In particular, the MP multi model ensemble has shown close agreement to proxy data in the eastern tropical Pacific.

2.3. Spatial patterns and temporal behaviour analysis

Our first approach to analyse ENSO and PDO in the MP is through computing the spatial-weighted leading empirical orthogonal function (EOF1) of the SST anomalies of the MP and PI simulations in the North Pacific and tropical Pacific regions to compare their differentiated behaviours. The North Pacific and the tropical Pacific regions we use are the same as the ones defined in the section above (2.2 Model evaluation). These spatial-weighted EOFs are normalised by their spatial standard deviations following Power et al. (2013), used in Brierley (2015) and Oldeman et al. (2021). The EOF calculation allows us to visually identify the main patterns of variability (regions with the largest loadings or temperature variability) in the Pacific basin and to analyse the characteristics of ENSO and PDO variability. We also perform spectral analysis of the principal components (PCs) of these two regions to analyse and compare their dominant frequencies.

The leading EOF for the whole Pacific basin is also analysed using the regions described in Section 2.2. Additionally, we perform a spectral analysis to obtain the dominant frequencies of the PC. For the spectral analysis, we use in all sections of this paper a multi taper spectral method with 10 tapers and a bandwidth of 6 with a previously normalised and detrended SST anomalies datasets, following Ghil et al. (2002), who suggested using more than 3 tapers in large datasets, such as centennial ones. We investigate whether the spectral power is significant at a 95 % confidence level. Confidence intervals have been computed using a first-order autoregressive (AR(1)) model with Monte Carlo generated surrogates, following the method by Oldeman (2021). The MMM for the spatial pattern was calculated by averaging the EOF1 for individual models. For the spectral analysis, the MMM was computed by first calculating the power spectrum and corresponding confidence intervals of the leading principal component (PC1) time series from each model individually and then averaging these spectra and confidence levels across all models.

2.4. El Niño and PDO indices analysis

We use two indices, one for ENSO and another for PDO. For ENSO, the Oceanic Niño Index (ONI) was calculated. This index is defined as the 3-month running mean of SST anomalies in the Niño 3.4 region (170° W–120° W; 5° S–5° N; e.g., Glantz and Ramirez, 2020). For the PDO, we computed the PDO index. This index is defined as the PC corresponding to the (spatial-weighted) first EOF of SST anomalies in the North Pacific basin (here, the same as the North Pacific region, 120° E–120° W; 20° N–70° N; Mantua et al., 1997).

The ONI and PDO indices were analysed in different ways based on their time series. Firstly, we calculated the amplitudes of the ONI and PDO indices by computing their standard deviation in the MP and PI. Then, we computed the relative changes in MP amplitudes compared to the PI. Secondly, we calculated correlations between ENSO and PDO in two ways. First, we calculated Pearson correlation coefficients between ENSO and PDO indices and statistical significance at p-value < 0.05. We also computed the relative changes in the MP compared to the PI. Second, we performed cross-correlations of the PDO and ENSO times series on a monthly basis for the entire period of each model. The MMM correlation coefficient was computed by averaging indices for ENSO and PDO retrieved for individual models and then calculating the cross-correlation.

3. Results

3.1. PlioMIP2 variance evaluation

The variance of the SST anomalies in the Pacific basin for MMM MP and PI, NOAA ERSSTv5 and the difference of variance MP-PI are shown in Fig. 1. The NOAA ERSSTv5 variance (Fig. 1a) is enhanced (i.e., has the highest variance) in two regions: in the tropical Pacific and the North Pacific, where we find enhanced variance in the PI and MP MMM (Fig. 1b and c). The NOAA ERSSTv5 tropical Pacific variance is large at the east, while the North Pacific variance is spread out. Differences are found in the PI and MP MMM (Fig. 1b and c, respectively), which exhibit a concentrated variance more to the west and central tropical Pacific than NOAA ERSSTv5 and a high North Pacific variance centred to the western North Pacific. Another difference based on NOAA ERSSTv5 is that the PI MMM variance is underestimated along the Bering Strait and the coast of North America, while it is overestimated in the tropical Pacific between around 130° W–100° W.

Variance in individual models is shown in Fig. S1. In general, the variance for individual models and MMM compare well to NOAA ERSSTv5, but there is a spread between them. COSMOS stands out due

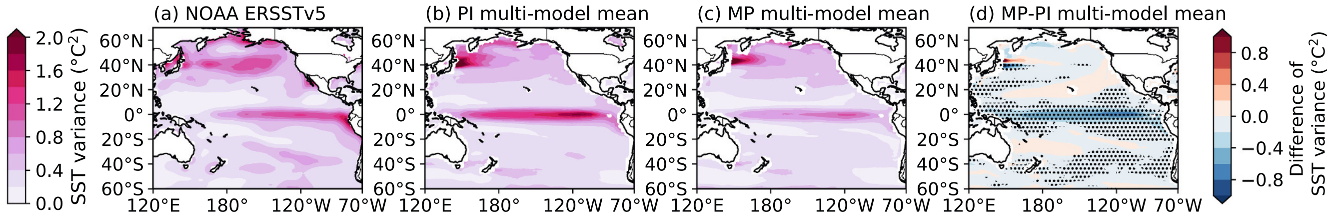

Fig. 1. MMM of SST anomalies (°C^2) in the (a) NOAA ERSSTv5 (reconstruction, 1870–2018), (b) PI MMM, (c) MP MMM and (d) the difference of the MMM variance (MP-PI). The stippling indicates areas where 5 or more models (~70 %) agree on the decease of variance in the MP compared to the PI.

to its relatively large variance (~2 °C^2) along the tropical Pacific in the PI and MP (Fig. S1c and j, respectively). MIROC4m also stands out due to the relatively small variability in the tropical Pacific (~0.6 °C^2) in the PI and MP (Fig. S1f and m, respectively).

The variance in the MP is reduced compared to the PI in the MMM (Fig. 1b, c and d) and in most individual models (Figs. S1 and S2). Compared to the PI, in the tropical region, the MMM MP variance (35 %) is much more reduced than in the North Pacific (8 %), as shown in Table 2 and Fig. 1d. Among models, in the MP North Pacific, HadCM3 shows a very increased variance (Table 2, Fig. S2d). Spatially, the difference in variance between the MP and PI (Fig. S2) reveals a general decrease of variance in the MP, with some models showing an increased MP variance located in the North or northeastern Pacific. The stipple shown in Fig. 1d indicates regions where at least 70 % of the models (5 out of 7 models) agree on the same direction of change of variance in the MP. These regions are mainly located in the tropical Pacific, implying that this is the region where most models agree on a decrease of variance in the MP.

3.2. *Analysis of the tropical Pacific and North Pacific regions*

In this section, we analyse the spatial and temporal properties of the SST anomalies in the MP compared to the PI. We show the spatial patterns and spectral analysis in the tropical Pacific and North Pacific regions separately, as well as in the whole Pacific basin. Plots shown in this section are divided into three columns, where the first column shows results from MP simulations including the MMM (letters a–h), the second column shows results from PI simulations including the MMM and the observational reconstructed NOAA ERSSTv5 for reference (letters i–q) and the third column (letters r–z) shows the power spectra of variability (periodograms) for the MP, PI and the observational reconstruct. In this study, we focus our analysis on the EOF1 and the first principal component (PC1) only, which represent the most relevant component of variability.

3.2.1. *The spatial patterns in the tropical Pacific and North Pacific regions*

Spatial patterns of EOF1 in the tropical Pacific show an ENSO pattern in all models in MP and PI simulations (Fig. 2 a–p). The PI simulations show a similar pattern to the NOAA ERSSTv5 (Fig. 2q), although the simulated ENSO pattern is extended to the central and west tropical Pacific in all models and the SST variability is underestimated in the eastern tropical Pacific. The tropical Pacific patterns of the MP vary slightly from the PI mainly in two ways. First, patterns are slightly extended polewards in 5 models (CCSM4-Utr, CESM1.2, HadCM3, MIROC4m and NorESM-L) and the MMM. This meridional elongation in the MP ENSO patterns is similar to that found in the multi model ensemble on an interannual scale of PlioMIP2 (Oldeman et al., 2021) and PlioMIP1 (Brierley, 2015). Second, 4 models (CCSM4-Utr, CESM1.2, HadCM3 and IPSLCM6A-LR) show that the ENSO pattern is zonally extended. Depending on the models, this zonal elongation is extended to the east, west, or both sides; however, most models show a pattern slightly shifted to the west. This westward shift is also found in the PlioMIP1 HadCM3 model on a multi centennial scale (Tindall et al., 2016).

The percentage of the variance explained by the first EOF is mostly reduced in the MP (Fig. 2, numbers on the top right of each figure). Our results show a decrease of the percentage of the variance explained (by 10 %) in the MP MMM, and also a decrease in most models, albeit with a large spread of change among them. Oldeman et al. (2021) showed a decrease in the MP MMM of 8 % with 14 out of 17 models, which is consistent with our results despite using more extended simulations' datasets. Between single models, in CCSM4-Utr the first EOF explains a much lower proportion of the variance in the MP compared to the PI (a difference of 31 %).

The spectral analysis of the leading EOF in the tropical Pacific shows peaks of power on multi annual and decadal time scales (Fig. 2 r–z). The MMM indicates that the peak of power is located between 5 and 6 years both in PI and MP simulations. In most models, significant portions of the power spectra (i.e., exceeding the 95 % confidence, shaded areas) indicate that the significant spectral peaks occur mostly on a multi annual time scale of 2–7 years, consistent with ENSO variability. A detailed analysis on an interannual time scale can be found in Oldeman et al. (2021), where no clear shift to lower frequencies was found in the MP. On a decadal time scale, NOAA ERSSTv5 does not show significant power. Similarly, the majority of the models show no significant power, both in the PI and MP. However, we do observe some important peaks at low frequencies (≥10 years) in the MP in 4 models (CCSM4-Utr, HadCM3, MIROC4m and NorESM-L). Moreover, a clear shift of power peaks from an interannual scale in the PI to a decadal scale in the MP is shown in HadCM3.

In the North Pacific region, all models and simulations show that the first EOF of SST variability has the typical horseshoe pattern of PDO (Fig. 3 a–q) with only small differences between models. In general, the PI models compare well with the NOAA ERSSTv5 data. Patterns in the PI and MP are very similar.

The percentage of the variance explained by the first EOF in MP, that we attribute to PDO, is similar to the PI in the MMM (Fig. 3, numbers on the top right of each figure). We find that in 3 models (CESM-1.2, COSMOS and HadCM3), the percentage of variance in the North Pacific increases. This increase is also reflected in the MP MMM (by 2 %). Meanwhile, CESM4-Utr shows a decrease, and other models show only minor changes. Compared to the tropical Pacific region, in both

Table 2
Variance change (MP-PI) in the PlioMIP2 PI simulation models and MMM in the tropical Pacific (150°E–80°W; 20°S–20°N), North Pacific (120°E–120°W; 20° N–70° N) and the whole Pacific (120° E–70°W; 60°S–70°N).

Model	Relative change of variance (%) in the tropical Pacific	Relative change of variance (%) in the North Pacific	Relative change of variance (%) in the whole Pacific
CCSM4-Utr	−70	−39	−46
CESM1.2	−46	2	−22
COSMOS	−20	−10	−14
HadCM3	−16	30	7
IPSLCM6A-LR	1	−9	−9
MIROC4m	−41	−8	−21
NorESM-L	−56	−23	−37
MMM	−35.4	−8.1	−20.3

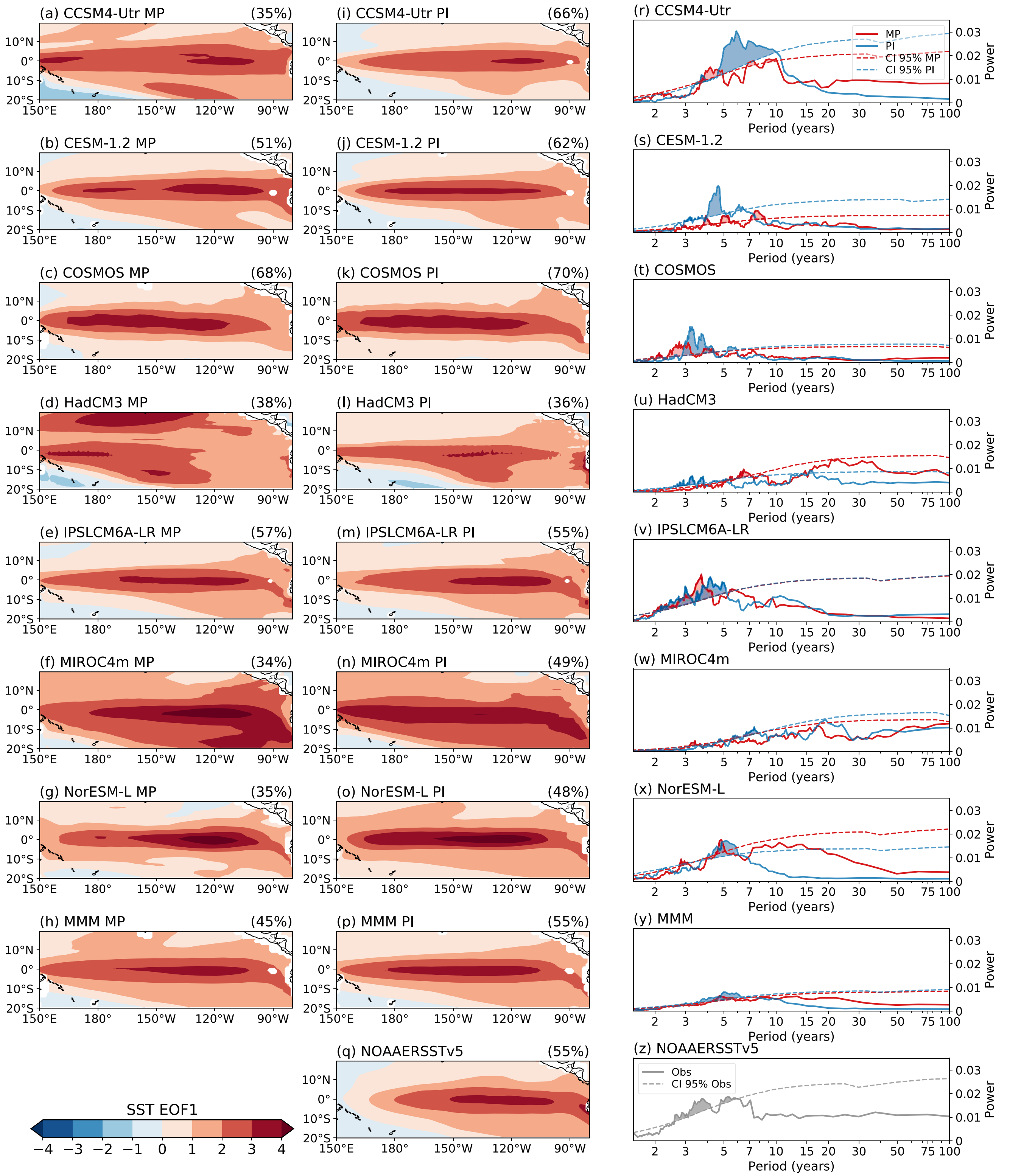

Fig. 2. Spatial patterns obtained from EOF1 of SST anomalies over the tropical Pacific region in the MP and PI simulations of all 7 considered PlioMIP2 models and their MMM. For each model, the variability explained by the EOF1 is shown in brackets. The right column (r–z) shows the periodograms of the EOF1 in the MP (red), PI (blue) and the observational reconstruct (grey). Dashed lines in the periodograms indicate the 95 % confidence level, while shaded areas in the periodograms indicate power spectra above the 95 % confidence level. (For interpretation of the references to color in this figure legend, the reader is referred to the web version of this article.)

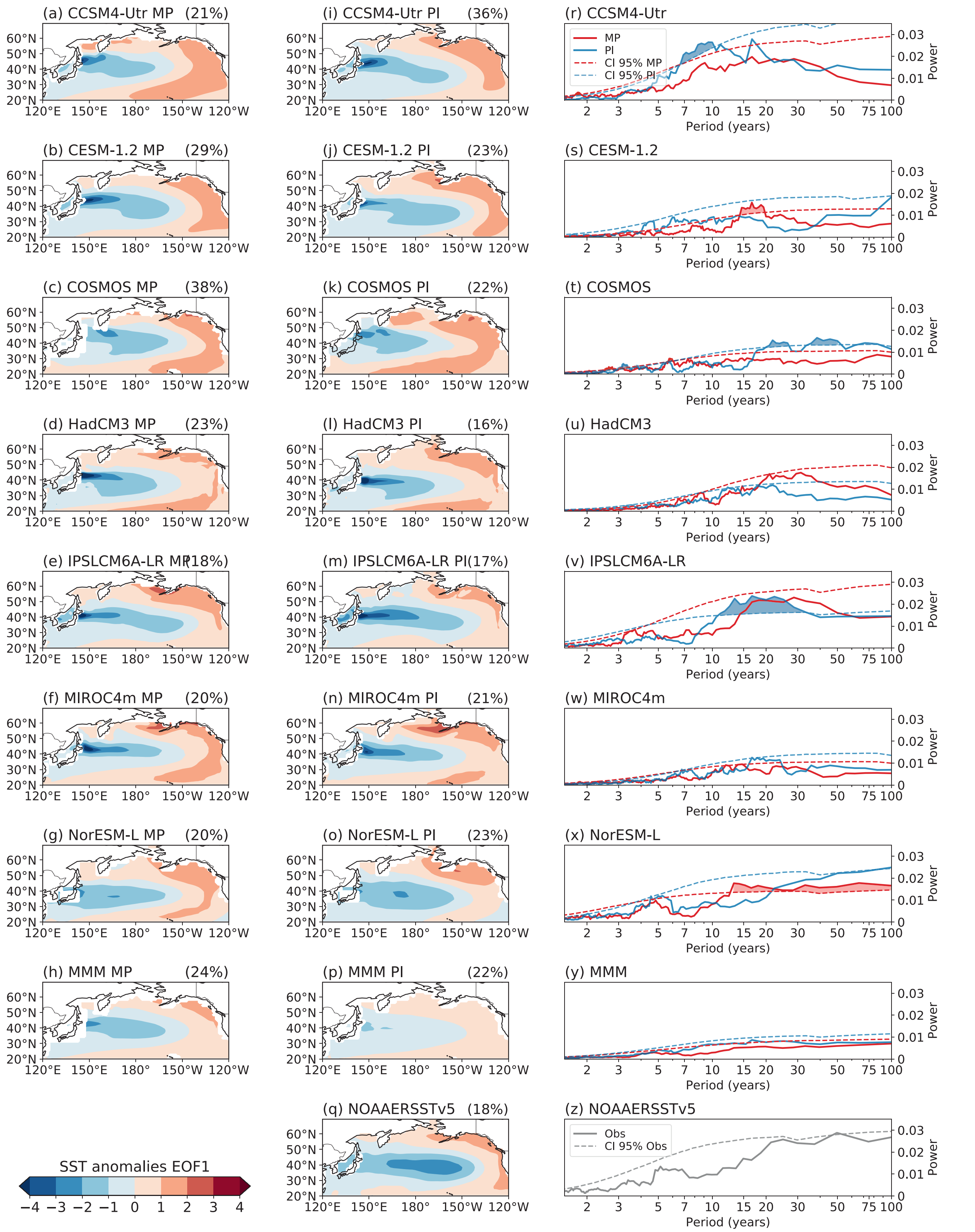

Fig. 3. Spatial patterns obtained from EOF1 of SST anomalies over the North Pacific region in the MP and PI simulations of all 7 considered PlioMIP2 models and their MMM. For each model, the variability explained by the EOF1 is shown in brackets. The right column (r–z) shows the periodograms of the EOF1 in the MP (red), PI (blue) and the observational reconstruct (grey). Dashed lines in the periodograms indicate the 95 % confidence level, while shaded areas in the periodograms indicate power spectra above the 95 % confidence level. (For interpretation of the references to color in this figure legend, the reader is referred to the web version of this article.)

simulations, the variance explained by the leading EOF in the North Pacific region is smaller by around half.

The spectral analysis in the North Pacific region indicates power peaks on a decadal scale, consistent with the PDO variability (Fig. 3 r–z), with some models showing changes towards lower frequencies in the MP. NOAA ERSSTv5 shows a non-significant peak at 25 years and a peak at 50 years that is just significant. However, due to this dataset's limited length (shorter than 200 years), these frequency peaks should be interpreted with caution, as the dataset may not reliably capture low-frequency variability. In contrast, frequencies in PI simulations are higher than those observed in NOAA ERSSTv5, peaking at 15–30 years mostly. The MMM shows that spectral power lines are overall flat, with barely noticeable peaks located between 18 and 30 years in both PI and MP simulations. Compared to the PI, some models show in the MP a power increase on a decadal scale (e.g., CESM-1.2, HadCM3). Conversely, other models show a decrease of power in this frequency range (e.g., COSMOS or CCSM4-Utr). One prevalent behaviour in the power spectra is that in 5 models (CESM-1.2, COSMOS, HadCM3, IPSLCM6A and MIROC4m), the MP shows their highest peaks at lower frequencies than in the PI, with a shift from about 10–25 to about 15–30 years. Although only in the case of HadCM3 and NorESM-L there is significance on this decadal period.

3.3. The main spatial pattern in the whole Pacific basin

Before exploring the differences between MP and PI variability, we focus on the agreement of PI simulations with the reconstructed observations. The leading Pacific basin EOF of the MP and PI simulations shows two main spatial patterns in the tropical and North Pacific, as does the NOAA ERSSTv5 reconstruction (Fig. 4 a–q). Nevertheless, we observe some differences between the PI MMM and the NOAA ERSSTv5 reconstruction data. Firstly, the tropical Pacific pattern of positive loadings (or temperature variability) in EOF1 along the equator extends too far to the west in the PI MMM and in every individual model. The distribution of this pattern in meridional direction has large spread, where some models show a too narrow tongue, and some show one that is too wide. The MMM captures the meridional extent of the observational pattern relatively well, suggesting that individual model biases seem to cancel out each other relatively well. Secondly, the simulated PI signal in the North Pacific is slightly weaker than the observed one, with several models (CCSM4-Utr, HadCM3, and MIROC4m) being relatively close to observations. Despite those differences between PI simulations and observations, models and their MMM capture important characteristics and the main signals of variability in EOF1 of the Pacific basin.

Some of the MP simulations and MMM show interesting differences in the main patterns compared to PI simulations. The MMM MP shows that the North Pacific pattern becomes more important than in the PI (Fig. 4 h and p, respectively), as the MMM MP shows large loadings in this region. However, this North Pacific pattern does not have the largest loadings of the whole Pacific basin in all models, as the pattern with the largest loadings still located (although reduced in comparison to the PI) in the tropical Pacific. Among models, we observe two different behaviours, and we group them accordingly: group I (CCSM4-Utr, CESM-1.2, HadCM3 and MIROC4m) and group II (COSMOS, IPSLCM6A and NorESM-L). Models in group I show a pattern with increased loadings in the North Pacific and a pattern with decreased loadings in the tropical Pacific compared to the PI. Furthermore, for 3 models in group I (CCSM4-Utr, HadCM3, and MIROC4m), the main pattern of the Pacific in the MP is located rather in the North Pacific than in the tropical Pacific. Conversely, in group II, differences in loadings of the MP patterns are minor compared to the PI (especially in COSMOS and IPSLCM6A). In this group, the tropical Pacific pattern is still the main pattern in the Pacific basin in the MP (similar to the PI) with a damped North Pacific loading.

Patterns of the whole Pacific basin show differences compared to patterns for the isolated North Pacific and tropical Pacific regions shown in Fig. 2 and Fig. 3, respectively. Patterns found in the whole Pacific basin (Fig. 4) show that, compared to the PI, the tropical Pacific has reduced loadings in EOF1. In contrast, when analysing the isolated tropical Pacific region, the tropical Pacific does not show this decrease. In addition, when analysing the whole Pacific basin, the North Pacific shows an enhanced MP North Pacific pattern. Conversely, there is no large change in the isolated North Pacific region.

It appears that for MP simulations, EOF1 of the whole Pacific region explains less temperature variability. The percentage of variance explained by EOF1 decreases in the MP simulations (Fig. 4, numbers on the top right of each figure). For the MMM, this percentage of variance is smaller in the MP than in the PI (by 7 %). In group I models (except HadCM3), this percentage of variance in the MP is much smaller than in the PI, especially in CCSM4-Utr and CESM-1.2. In contrast to group I, group II models show only small changes. Compared to the percentage of variance explained in the MP tropical Pacific (reduced in the MMM) and the MP North Pacific (slightly increased in the MMM) regions, the percentage of variance of the MP for the whole Pacific basin is reduced and close to that found in the North Pacific region.

When focusing on the frequency of variability of the entire Pacific basin, we find that the NOAA ERSSTv5 reconstruction shows significant peaks on an interannual scale (3–6 years). The MMM PI simulations show a similar power behaviour to NOAA ERSSTv5 in the periodicity between 5 and 6 years. When comparing the frequencies between models (Fig. 4 r–y), we find appreciable differences in the dominant peaks between groups I and II. In the MP, power peaks shift to lower frequencies (longer periods) in the MMM, in group I models (CCSM4-Utr, CESM-1.2, HadCM3) and in NorESM-L. In these models, we find the dominant peaks on a decadal time scale, between 15 and 35 years, representing a dominant decadal frequency, typical of PDO frequency. Note that most power in low frequency variability is not significant above the 95 % confidence level. On the contrary, two of the models of group II, COSMOS and IPSL–CM6A, show a MP dominant power peaking at interannual frequencies (3–5 years), very similar to the variability simulated for the PI.

Compared to PI, power peaks in the MP shift to lower frequencies (longer periods) in the MMM. In group I models (CCSM4–Utr, CESM-1.2, HadCM3) and NorESM-L, we find the dominant peaks on a decadal time scale, between 15 and 35 years, representing a dominant decadal frequency, typical of PDO frequency. On the contrary, COSMOS and IPSL-CM6A show a MP dominant power peaking at interannual frequencies (3–5 years), very similar to the PI. On the other hand, MIROC4m shows increased power on a decadal scale in MP and PI, with peaks between 15 and 25 years in both simulations. Compared to the spectral power of the solely tropical and North Pacific regions, in the Pacific basin we find similar results to that found in the PDO with a shift to lower frequencies in the MP. On the other hand, MIROC4m shows increased power on a decadal scale in both MP and PI simulations, with peaks between 15 and 25 years in both simulations. Compared to the spectral power found when analysing variability in the isolated tropical and North Pacific regions, our results for the entire Pacific basin are similar to that found in the PDO, with a shift to lower frequencies in the MP.

3.4. ENSO and PDO indices analysis

We calculated the amplitude of the ONI and PDO indices to understand the differences in the SST behaviour observed in Sections 3.2 and 3.3. As previously described in Section 2.4, here we analyse ENSO and PDO amplitudes represented by the ONI and PDO indices, respectively.

ONI amplitudes are reduced in the MP in comparison to PI simulations (Fig. 5). Compared to NOAA ERSSTv5, PI models show similar amplitude, although COSMOS shows a large overestimation. The ONI MMM amplitude is decreased in the MP (by 30 %) compared to PI. All models except IPSLCM6A show a reduced amplitude in the MP. CCSM4-Utr stands out because of its large amplitude reduction (by 68 %). Overall, our results coincide with results found in Oldeman et al. (2021),

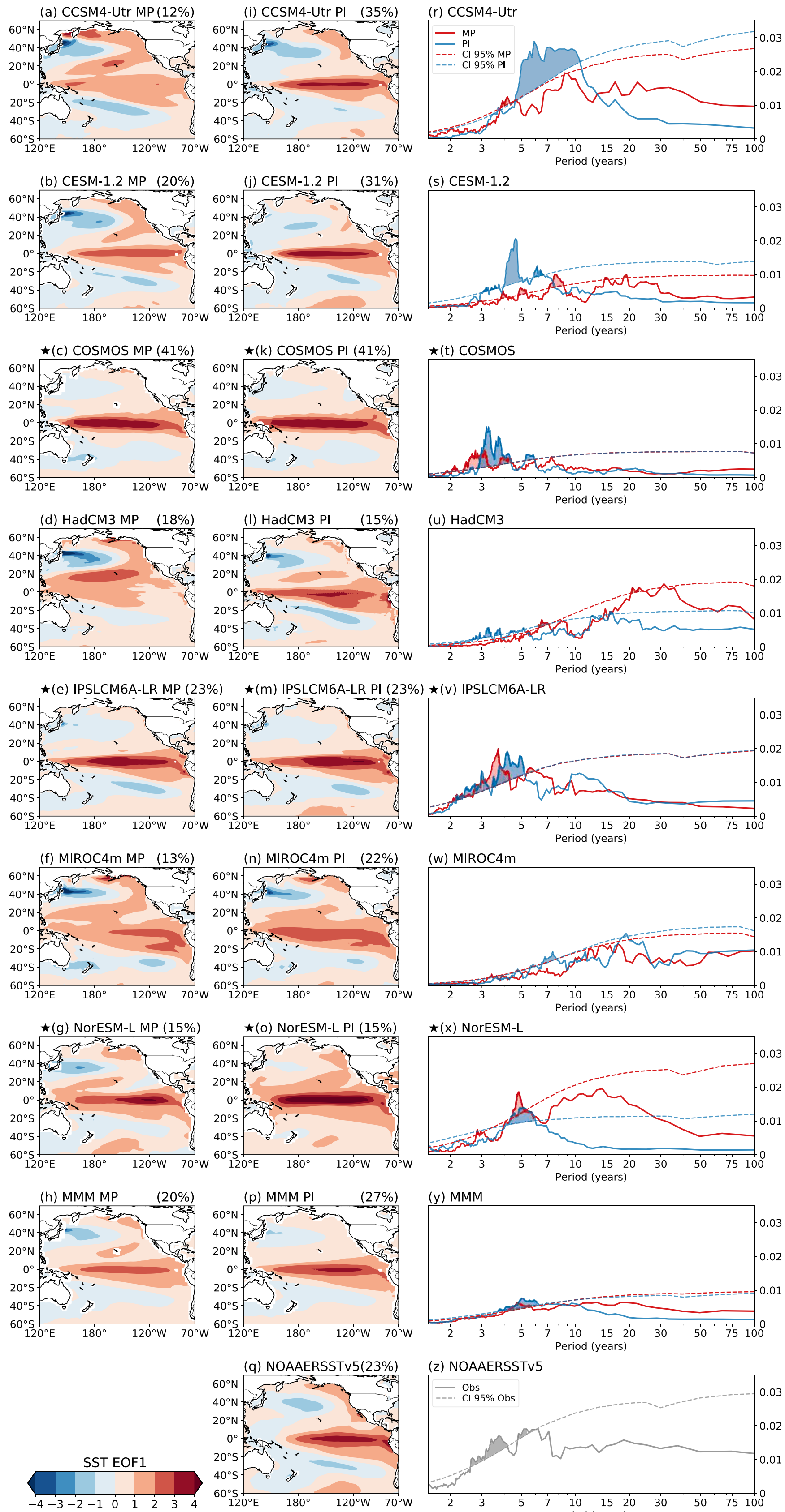

(caption on next page)

Fig. 4. Spatial patterns obtained from EOF1 of SST anomalies over the Pacific basin in the PlioMIP2 MP and PI simulations of all 7 considered PlioMIP2 models and the MMM. The variability explained by the EOF1 in each model is shown in brackets. The right column (r-z) shows the periodograms of the EOF1 in the MP (red), PI (blue) and the observational reconstruct (grey). Shaded areas indicate power spectra above the 95 % confidence level. Models from group II are denoted with a ★, while the rest of them correspond to group I. (For interpretation of the references to color in this figure legend, the reader is referred to the web version of this article.)

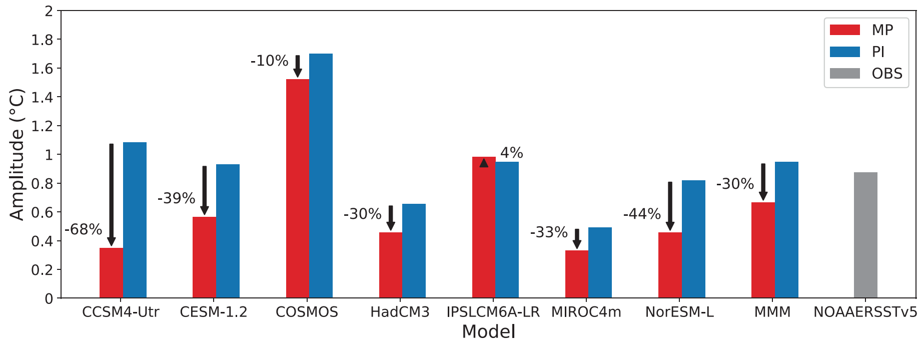

Fig. 5. Amplitudes of the ONI in the MP, PI and NOAA ERSSTv5. Numbers indicate the percentage change of amplitude (MP-PI). Arrows denote the magnitude of these changes in the MP indicating increases (upward) or decreases (downward) with relation to PI simulations.

who show an ONI amplitude reduction in 15 out of 17 models, with an ensemble mean decrease of 24 %. Furthermore, our results show a general amplitude reduction by 10–68 %, which coincides with the unanimous reduction by 10–55 % in amplitude in the MP found in Brierley (2015) using PlioMIP1 model simulations.

Amplitudes of the PDO index show only small changes in most models and there is no clear consistency of the differences between the MP and PI (Fig. 6). PDO amplitudes in the PI are mostly similar to that of NOAA ERSSTv5, except for CCSM4-Utr, which largely overestimates it. The MMM indicates no change in amplitude between MP and PI. Nevertheless, individual models show increases or decreases of PDO variability. More than half of the models (CCSM4-Utr, IPSLCM6A, MIROC4m and NorESM-L) indicate a PDO mean amplitude reduction of 17 % in the MP. On the contrary, the other 3 models (CESM1.2, COSMOS and HadCM3) indicate an increased mean amplitude of PDO of 23 % in the MP. Largest changes in amplitude are seen in CCSM4-Utr (−42 %). Brierley (2015) also showed increases and decreases in PDO amplitudes in PlioMIP1 models.

The MP ENSO shows larger and more consistent changes in amplitude than the PDO does. A clear amplitude reduction in the MP is shown in 6 out of 7 models. Yet, PDO amplitude changes between the MP and PI do not have a clear direction of change. One might suspect that these differences between ENSO and PDO could be related to the nature of the index used. While the ONI is based on the direct use of SST anomalies in the tropical Pacific region, the PDO index is based on the first PC in the North Pacific region. As a way of contrasting the possible difference in the nature of the index, we computed the amplitude of variability in the El Niño 3.4 region (same region used by the ONI) using the SST anomalies' first PC (Fig. S3) and using a high-pass index following Wu and Liu (2020) in Fig. S4. We find that ONI amplitudes, amplitudes of the PC1 and amplitudes for the high-pass index in the tropical Pacific region show very similar changes in amplitude in the same direction. In addition, we used the low-pass SST anomalies index described by Wu and Liu (2020) to compute PDO amplitudes. Amplitude values and changes (MP-PI) using this index are generally smaller than using PC1. Even though a spread between models still exists, the MMM indicates little change. This way, we show that the nature of the index does not considerably impact our inferences of different behaviour between ENSO and PDO amplitude change between MP and PI simulations.

3.5. *ENSO and PDO correlations*

The Pearson correlation coefficients between ENSO and PDO, based on the ONI and PDO index, respectively, are shown in Fig. 7. The NOAA ERSSTv5 reconstruction shows a correlation coefficient of 0.35 between both modes of variability. PI simulations show reasonably similar correlation coefficients to NOAA ERSSTv5, although CCSM4-Utr and MIROC4m overestimate it. The MMM shows a larger correlation coefficient in the PI (0.3) than in the MP (0.24), corresponding to a decrease in correlations coefficients by 18 %. More than the half of the models (CCSM4-Utr, CESM-1.2, COSMOS and MIROC4m) show decreases in correlations in the MP, which are especially large in CCSM4-Utr (−63 %). Meanwhile, the rest of the models show increases, especially large in HadCM3 (39 %). The correlations between ONI and PDO index in both

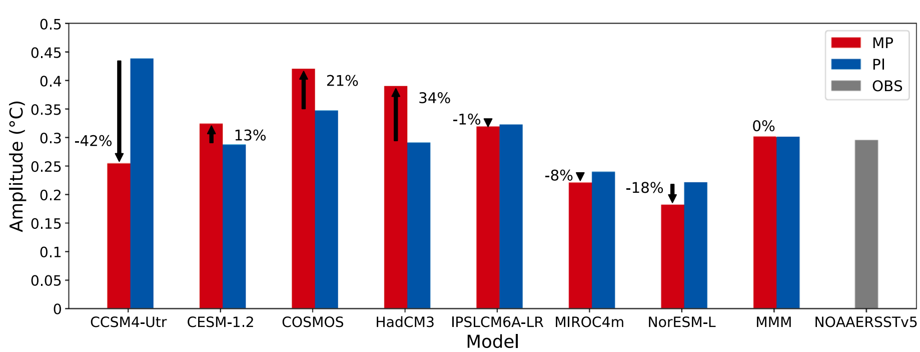

Fig. 6. Amplitudes of the PDO index in the MP, PI and NOAA ERSSTv5. Numbers indicate the percentage change of amplitude (MP-PI). Arrows denote the magnitude of these changes in the MP indicating increases (upward) or decreases (downward) with relation to PI simulations.

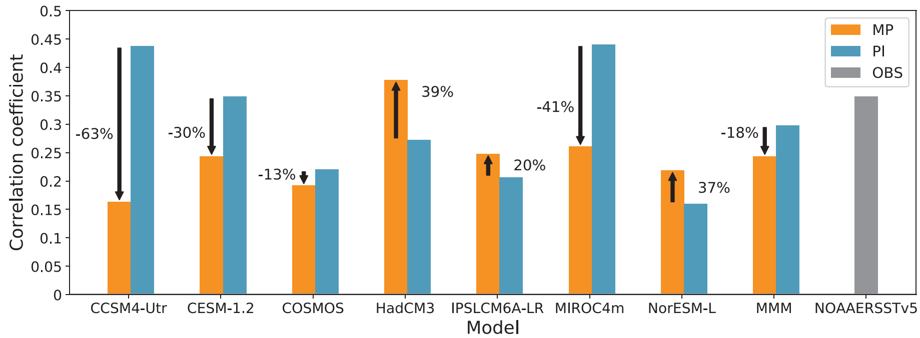

Fig. 7. Pearson correlation coefficients of the relationship between the ONI and the PDO index in the MP (orange bars), PI (blue bars) and NOAA ERSSTv5 (grey bar). Arrows denote the magnitude of these changes in the MP indicating increases (upward) or decreases (downward) with relation to PI simulations. All correlation coefficients are statistically significant (two-tailed p-value < 0.05). (For interpretation of the references to color in this figure legend, the reader is referred to the web version of this article.)

simulations are all statistically significant at *p*-value < 0.05.

Compared to ENSO-PDO correlation coefficients computed with observation for the recent climate (1900–2002), our results (Fig. 7) show small Pearson correlation coefficients. For instance, the correlation coefficient shown in Newman (2007) is around 0.7, while for NOAAERSSTv5, it is around 0.35. Meanwhile, for the MMM PI it is close to 0.3. These large differences compared to observations might be related to the fact that we detrended NOAAERSSTv5 so that recent warming trends affect as little as possible our results.

Results shown in Fig. 7 have some spread and do not show a consistent direction of change. To test if the nature of the index might play a role in this spread, we computed the Pearson correlation

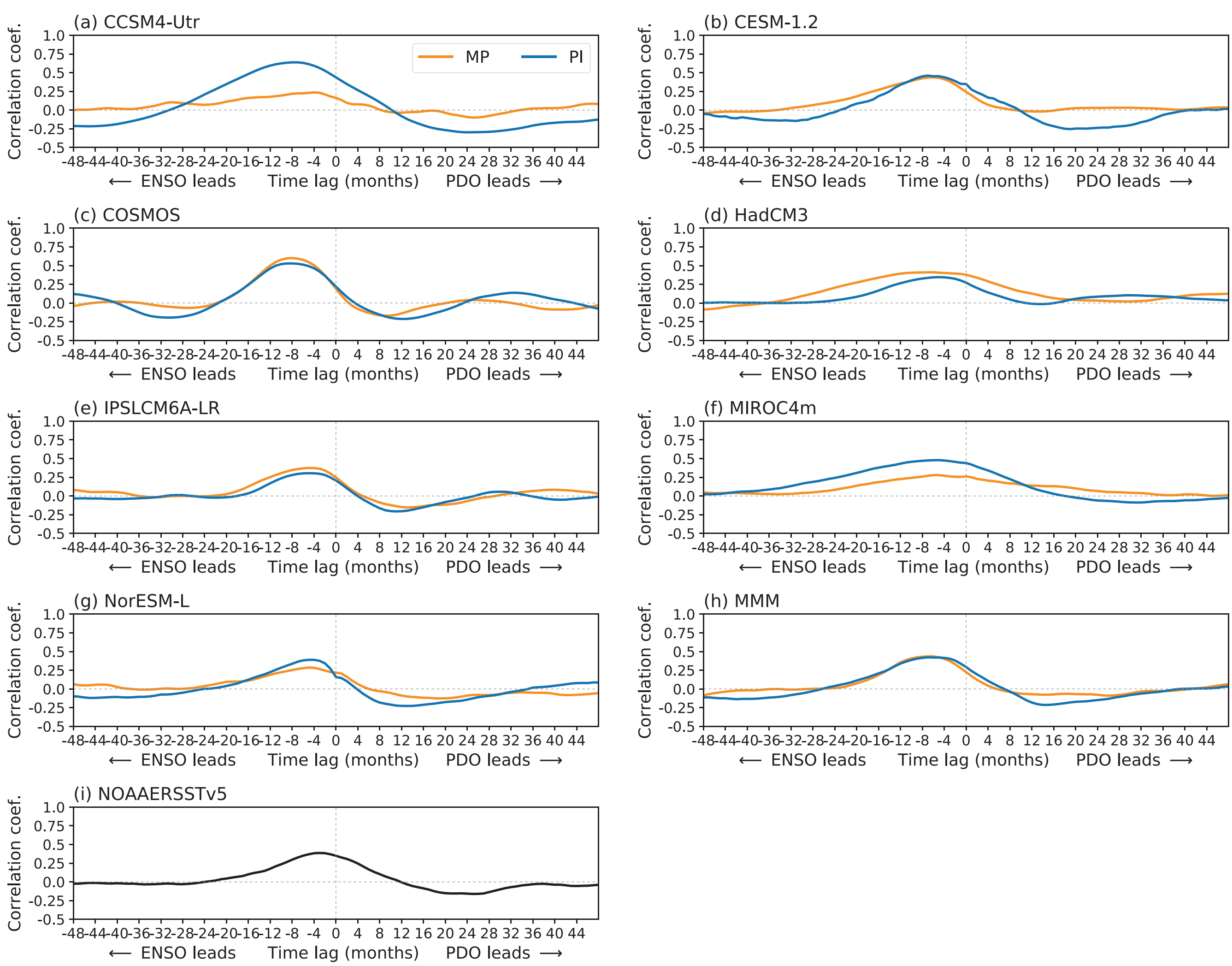

Fig. 8. Cross-correlation between the ONI and the PDO index in the MP (orange), PI (blue) simulations and the NOAA ERSSTv5 observational reconstruction (black). The lead/lag relation between ONI and PDO is indicated by arrows. (For interpretation of the references to color in this figure legend, the reader is referred to the web version of this article.)

coefficients of ENSO and PDO both based on the SST anomalies' PC1 (Fig. S6). We find similar values of correlation coefficients and the same direction of change. This way, we show that the nature of the index does not considerably impact our inferences of correlation changes between MP and PI simulations.

The mechanistic link between ENSO and PDO variability is explored through analysing the lagged correlation coefficients shown in Fig. 8. In all MP and PI simulations, ENSO leads PDO. In NOAA ERSSTv5, ENSO leads by 3 months and has a maximum lag correlation coefficient of 0.39. The MMM shows a very similar lag of PDO in the MP and PI simulations (5 months) and a maximum correlation coefficient of 0.45 in both simulations. In single models, we find lags of PDO with respect to ENSO of 4–8 months in the MP and PI simulations. Results for the MP HadCM3 (correlation coefficient of 0.38) are similar to that found in the PlioMIP1 HadCM3, as Tindall et al. (2016) found that PDO in the HadCM3 model has a higher correlation coefficient with ENSO in the MP than in the PI, and that ENSO leads PDO by ~6 months.

4. Discussion

4.1. PI model performance and groups formation

The PlioMIP2 PI MMM of the 7 models considered by us captures well the patterns of SST variance observed in the NOAA ERSSTv5 observational reconstructions (Fig. 1). Variance along the coast of South America is underestimated in the models. This underestimation might be related to the fact that (the variability of) coastal currents, upwelling and marine stratus cloud cover are not well resolved in the models, which is a known bias related to model resolution (Colas et al., 2012; Li and Xie, 2012; Ma et al., 1996). SST variability along the Bering Strait and Alaskan peninsula is also underestimated. Nevertheless, SST variability in the Arctic is strongly linked to sea-ice variability (Carvalho and Wang, 2020) and influenced by large scale SST variability via the AMOC (Vaideanu et al., 2023), which is different in recent decades than in the PI. It is worth remarking that any discrepancies could result from the fact that we are comparing PI simulations with reconstructed historical and PI data. Even if the latter have been detrended to remove the anthropogenic warming trend, an anthropogenic effect might still exist.

To assess any detectable differences between models, we define two groups based on EOF1 (Fig. 4). This grouping exercise helps us examine differences in model responses to forcing and sensitivity to better comprehend the spread of spatial patterns and frequencies. While our grouping is not fully consistent, possibly due to the small ensemble (only 7 out of 17 PlioMIP2 models), it still provides a useful comparison to past studies with more comprehensive classifications. For example, Oldeman et al. (2021) identified two SST-based groups: group A (including COSMOS, IPSLCM6A) and group B (including CESM4-Utr). Similar to our group II, group A showed no ENSO amplitude change and enhanced variability. Ren et al. (2023), using pattern correlations and hierarchical clustering, identified five clusters and a multi-cluster mean (MCM) instead of a MMM. Cluster 4 (with IPSLCM6A-LR, COSMOS) matches our group II, while clusters 2 and 3 (including MIROC4m, HadCM3, CESM1.2) align with our group I. So, we can see that PlioMIP2 models do show marked differences among groups in their response to Pliocene boundary conditions. Ideally, these differences should be quantified using appropriate methods as in Ren et al. (2023).

4.2. The dominant variability in the Pacific basin

In the MP Pacific basin, we find that models do not show a unanimous main pattern in the first EOF or similar frequencies (Fig. 4). Models in group II have a similar EOF1 in the MP and PI. Meanwhile, in group I models we find that the EOF1 main pattern in the Pacific is in the North Pacific, representative of the PDO. In the EOF1 MP of models in group I, a reduced strength in the tropical Pacific pattern and an enhanced North Pacific pattern is shown. Partially similar to our findings, a main pattern located in the North Pacific in the first and second EOF of MP simulations was previously found in the NorESM-L PlioMIP1 model, with no clear pattern in the tropical Pacific (Brierley, 2015). In addition, we find that the possible shift in the main pattern in the MP is accompanied by an increase in the dominant period from 3–5 years to 15–35 years, which suggests that the decadal scale variability (PDO) was dominant over the interannual scale variability (ENSO). A tendency of reduction of frequency (by 12 %) was also found previously in Tindall et al. (2016) for the HadCM3 PlioMIP1 model over a multi centennial scale.

MP amplitudes of ENSO and PDO indicate a weaker ENSO and no consistent changes in the PDO in comparison to PI simulations. In 3 models (CESM1.2, COSMOS and HadCM3), the amplitude of ENSO decreases in the MP while the amplitude of the PDO increases (Figs. 5 and 6). Meanwhile, in 1 model (MIROC4m), the ENSO amplitude decreases in the MP but the PDO amplitude remains similar (Figs. 5 and 6). Do these amplitude changes mean that the dominance of variability in the Pacific basin was different in the MP? The decrease in ENSO amplitude coincides with the reduced pattern of the tropical Pacific in the Pacific basin in group I models (Fig. 4). However, the large spread in MP PDO amplitudes does not necessarily coincide with an enhanced North Pacific pattern. This different behaviour in MP variability (compared to the PI) suggests that the MP PDO might have gained relative importance in the Pacific basin as ENSO amplitude decreased, even though PDO amplitude itself does not change much.

4.3. The ENSO-PDO relationship

In the present day climate, ENSO is known to lead PDO variability linearly on time scales of a few months primarily through atmospheric teleconnections and associated oceanic Rossby waves (Newman et al., 2016; Nidheesh et al., 2017). Here, we analyse the PDO and ENSO relationship through correlation coefficient analysis. For most models, the PI simulates a correct and similar lagged but slightly weaker linear connection between ENSO and PDO, compared to NOAA ERSSTv5.

In the MP, 6 models simulate a weaker ENSO variability (Fig. 5), yet the change in PDO variability is small. Since PDO is largely driven by ENSO through a linear process, we might expect that reduced ENSO amplitudes would lead to weaker linear relationship between ENSO and PDO reflected in reduced correlation coefficients. However, not all the models show decreases in the correlation coefficients. Only in 4 models (CCSM4-Utr, CESM-1.2, COSMOS and MIROC4m) we find smaller correlation coefficients between ENSO and PDO in the MP (Fig. 7). For these models, the ENSO amplitude is reduced, while the PDO amplitude either reduces or increases. On the contrary, in 3 models (HadCM3, IPSLCM6A and NorESM-L), the ENSO–PDO correlation coefficient increases, while ENSO amplitudes decrease or do not change much. HadCM3 is the only case of increased correlation in the MP, even though the ENSO amplitude decreases and the PDO amplitude increases. Even so, in general, the changes of correlation coefficient are in the same direction as changes in ENSO amplitude, suggesting that the linear relation between ENSO and PDO is reduced in the MP. By analysing the correlation coefficients, we examine how linearly ENSO and PDO are connected. The strength of this teleconnection was explored in Oldeman et al. (2024) and they found only a slight change in its strength.

Regarding the lagged correlations, results showed little difference. For the majority of models (5), the lag for which there is the maximum correlation is unchanged in the MP, with ENSO leading PDO by 4–8 months. These results suggest that the physical mechanism linking PDO variability to ENSO is similar in the MP and PI, despite ENSO being suppressed in the MP and the correlation coefficient being either reduced or increased.

In studies of future scenarios, the PDO is projected to decrease in amplitude (Geng et al., 2019; S. Li et al., 2020) or amplify (Liguori and Lorenzo, 2018), and the ENSO-PDO connection might become more in-phase with ENSO and more dependent on the ENSO amplitude (Kwon et al., 2013; Nidheesh et al., 2017). In PlioMIP2, we find that the MP amplitude of PDO variability is largely unchanged compared to the PI (Fig. 6), and its correlation with ENSO is reduced (Fig. 7). These findings are consistent with results using the earlier PlioMIP1 ensemble (Brierley, 2015). However, previous work and our study illustrate that the PDO does not respond similarly to MP and future boundary conditions. We suspect that one of the reasons for this contrast in variability change between the MP and the future might be related to a different global climate equilibrium state: while PlioMIP2 MP simulations assume a long-term quasi-equilibrium, all the analyses for future scenarios cited here are based on transient states. In other words, quasi-equilibrium refers to a climate state in which the Earth had already adjusted or is nearly adjusted to changes in external forcings (e.g., CO_2 changes, orbital parameters, etc.). In contrast, a transient climate state reflects one still undergoing change not yet in equilibrium (e.g., King et al., 2020; Sherwood et al., 2020; PALAEOSENS Project Members, 2012).

4.4. Possible physical mechanisms

In the present day, the PDO is forced by different climate features. First, ENSO forces PDO variability primarily through atmospheric teleconnections, which transmit tropical signals to the extratropics via the atmospheric bridge (Alexander et al., 2002). These teleconnections affect the AL and associated North Pacific wind stress, expressed through the Pacific–North American (PNA) pattern (e.g. Di Lorenzo et al., 2013; Newman et al., 2016). Second, the PDO exhibits a re-emergence mechanism, where subsurface ocean temperature anomalies persist and resurface seasonally (Newman et al., 2016). Third, extratropical atmospheric stochastic variability, particularly in the AL, contributes to PDO variability independently of ENSO. Finally, oceanic Rossby waves play a role by contributing to long-term adjustments in ocean heat content and SST patterns in the North Pacific. Oldeman et al. (2024) investigated the ENSO–AL teleconnection in the PlioMIP2 in more detail and found that the variability of the MP AL is similar to PI (although with appreciable spread throughout the ensemble), despite ENSO being weakened. They found that, similar to the present day, the dominant forcing of the AL variability is internal atmospheric variability and not ENSO. This internal variability does not change significantly in the ensemble mean, leading to little or no overall change in the AL, even though ENSO is weakened.

How can we explain a similar PDO variability despite a substantially suppressed ENSO? The explanation is possible by considering a similar reasoning to the AL variability described in the previous paragraph. In both simulations, MP and PI, the correlation coefficient between ENSO and PDO is close to 0.3 (Fig. 7), which means that ~30 % of the magnitude of PDO variability is explained directly by ENSO, whereas the rest, ~70 %, is not. The majority of that forcing is related to the variability of the North Pacific atmosphere (i.e., the variability of the AL; e.g., Newman et al., 2016; Nidheesh et al., 2017), which is similar to the PI in the MP ensemble mean (Oldeman et al., 2024). Other features can impact the behaviour of PDO variability, such as possible changes in the AL–PDO teleconnection strength (e.g. via the impact of winds on SSTs) or changes in the ENSO–PDO teleconnection strength (e.g. related to the speed of ocean waves). Furthermore, the re-emergence mechanism of the PDO is not investigated in this study.

Even though we can explain the main features of MP SST variability in the Pacific Ocean in the PlioMIP2 ensemble mean, not all models simulate ENSO suppression and similar PDO with relation to the PI. For example, CCSM4-Utr simulated the largest ENSO and PDO suppression. HadCM3 simulated a substantial ENSO suppression but a substantial increase in PDO amplitude. Meanwhile, IPSLCM6A shows no important change overall. Possible reasons to explain some of the spread in the ensemble in the ENSO and the AL response are explored in Oldeman et al. (2024). They analysed the relative model sensitivity to either CO_2 increases or boundary conditions (e.g. closed Arctic gateways, including the Bering Strait, and reduced ice sheet extent). They found out that models with different sensitivities will have a different atmospheric response, which will influence the PDO variability in different ways, despite the unison response of ENSO.

To verify whether the mechanism of the PDO variability obeys CO_2 increases in the MP, we used a PlioMIP2 sensitivity experiment designed to test the impact of this forcing. In specific, we used the E^{400} simulation, which was run with equal configurations as in E^{280} (in particular, with PI geography), except for CO_2 atmospheric concentrations, which are set to 400 ppm (Haywood et al., 2016). We calculated the leading EOF for 6 PlioMIP2 models for 100 years. These models are CCSM4-UoT (Chandan and Peltier, 2017), CESM2 (Feng et al., 2020), COSMOS (Stepanek et al., 2020), HadCM3 (Hunter et al., 2019), MIROC4m (Chan and Abe-Ouchi, 2020) and NorESM1-F (X. Li et al., 2020). We used this small number of models and for a reduced period because only these PlioMIP2 models conducted the E^{400} simulation, with data availability for 100 years. Results indicate that the Pacific Ocean SST variability in the E^{400} experiment has very similar patterns to the PI (Fig. S7). Moreover, when comparing results from the MP simulations to those from the E^{400}, patterns are very similar to that found in Fig. 4. Consequently, elevated CO_2 does not seem to be the main driver of PDO changes in the MP, but rather other Pliocene boundary conditions, such as land-sea mask changes and differences in ice sheets seem to have stronger relevance for PDO.

Our hypothesis that land-sea mask and ice sheet configuration might be the main drivers of the PDO variability in the MP is also reinforced by previous studies that assessed the model sensitivity within PlioMIP. Samakinwa et al. (2020) compared the effects of the different paleogeography in PlioMIP1 and PlioMIP2 (PRISM3D and PRISM4, respectively) for COSMOS. They found that paleogeography is an important driver that influences SST warming, especially in the Arctic. Using the CCSM4 model to develop sensitivity experiments, Otto-Bliesner et al. (2017a) found that, due to the closure of the Bering Strait and Canadian Arctic Archipelago, less North Pacific freshwater reaches the Arctic Ocean in the Pliocene, causing a warmer SST in the North Atlantic. In general, the gateway and ice sheet configuration are important drivers of climate. However, the specific mechanics of their influence over PDO may vary between models. Further insight into the mechanisms is limited by the absence of sensitivity simulations, which could allow to have more comprehensive understanding of changes in individual gateways with different boundary conditions.

Lastly, the response of the MP PDO could also be related to the response of the Arctic climate. Recent work has shown that the PDO has a complex relationship with Arctic sea-ice variability and regional atmospheric circulation (Kim et al., 2020; Simon et al., 2022; Yang et al., 2020). The PlioMIP2 models simulate a substantially warmer MP Arctic with a corresponding substantial reduction in sea-ice extent, and most models simulate sea-ice free conditions in summer (De Nooijer et al., 2020). Arctic climate changes, particularly polar amplification, which has a model-dependent factor (Haywood et al., 2020), can influence the variability of the PDO, and climate variability in different climate models can therefore have different sensitivities to those changes. However, exploring the relationship between Arctic sea-ice and PDO changes in the MP goes outside of the scope of this work.

All analyses and results presented here were performed using simulations from PlioMIP2 models. Given the spread between models, the outcomes from our analyses should be revisited in the future, ideally with a larger model ensemble and considering additional sensitivity simulations. Our results and the inferences we made from our analyses are still valid for PlioMIP3, which employs the same core experiments as PlioMIP2 (Haywood et al., 2024). Models and simulations developed since then should be analysed considering any boundary condition changes.

4.5. Advances in understanding the climate over the Pacific basin with PlioMIP models

Our results are part of an ongoing advancement in the comprehension of ENSO and related dynamics in the MP. We show a reduction of ENSO amplitude based on 200–500 year of PlioMIP2 simulations, which agrees with results based on 50–100 years of PlioMIP2 simulations (Oldeman et al., 2021; Pontes et al., 2022), as well as with results from the PlioMIP1 ensemble (Zhang et al., 2012; Brierley, 2015). We also observe a slight meridional expansion and westward shift of ENSO's centre of gravity, which could be related to the westward shift of the Walker Circulation (Han et al., 2021) and the enhanced easterly wind stress in the west Pacific (Ren et al., 2023) as reported in previous studies using the PlioMIP2.

Recent advances in understanding the PDO and its relationship with ENSO during the MP reveal some changes from previous studies. A stronger PDO and a robust linear ENSO-PDO relationship in the MP PlioMIP1 HadCM3 model was shown by Tindall et al. (2016), which align with our results for PlioMIP2 HadCM3. Conversely, Brierley (2015) found no consistent changes in PDO amplitude, frequency or spatial patterns across the PlioMIP1 ensemble, while our PlioMIP2 results show smaller changes in PDO amplitude. This discrepancy may relate to the Bering Strait configuration, which shifted from open in PlioMIP1 to closed in PlioMIP2. More recently, Oldeman et al. (2024) used the PlioMIP2 ensemble to examine the AL, finding that its variability was primarily driven by internal atmospheric processes, despite a weak ENSO.

In our analysis, we show a robust ENSO amplitude, yet PDO variability remains comparable to the PI, though not consistently across models. Frequencies tend to be of lower, towards decadal, and while the ENSO-PDO physical connection persists, their linear correlation weakens in the MP. Notably, model spread of amplitudes is in general greater in the North Pacific than in the tropical Pacific across PlioMIP simulations. This variability highlights the importance of sensitivity studies for different orographic configurations, atmospheric CO_2 levels, and gateway changes. In particular, the closure of the Bering Strait. Future studies should also consider how spatial ocean resolution may influence circulation responses to those boundary condition changes.

5. Summary and conclusions

The ENSO and PDO were analysed in the mid-Pliocene warm period (MP), an interesting geological time to study due to the increased CO_2 atmospheric concentrations (400 ppm, similar to modern) and 2–3 °C warmer mean global temperature than in the pre-industrial (PI). In this study, we used centennial SST from an ensemble of 7 models from the Pliocene Model Intercomparison Project phase 2 (PlioMIP2). We investigated changes in the ENSO and PDO behaviour in the MP. For that purpose, we analysed the leading EOF and other variability properties (variance, spatial patterns, frequencies, amplitudes and correlations). We did not only focus on the Pacific basin as a whole but also applied our analyses on two isolated regions: the North and tropical Pacific.

SST anomaly patterns in the MP over the whole Pacific basin are considerably different in comparison to isolated patterns in the tropical and North Pacific regions. In the isolated tropical Pacific, the ENSO pattern is similarly represented in the MP and PI simulations in all models and the multi model mean (MMM), although there are small changes, such as meridional and/or western shifts or elongations in patterns of single models (Fig. 2). In turn, the isolated North Pacific pattern is similarly represented in the MP and PI (Fig. 3). Conversely, in the whole Pacific basin, the tropical region has a reduced pattern in 4 out of 7 models, while patterns in the North Pacific (representing the PDO) gained importance in the same models (Fig. 4). Moreover, in 3 out of 7 models, PDO becomes the main pattern in the Pacific Ocean.

EOF analyses used to observe changes in spatial patterns are useful mathematical tools but their results should be carefully interpreted, as they could misinform physical processes (e.g., inaccurate centres of action; Dommenget and Latif, 2002). Consequently, results obtained from EOFs are only indicative. Even with this caveat, the spectral analysis of the first PC shows a shift of frequency for 4 out of 7 models, which decreases from interannual (3–5 years) to decadal (15–35 years), suggesting that in the MP decadal scale variability (PDO) is predominant over the interannual scale variability (ENSO). Furthermore, when analysing the amplitude of ENSO and PDO, we find that MP ENSO amplitudes are largely decreased (by 30 % in the MMM) with a robust weakening ENSO relative to the PI in most (6 out of 7) models but PDO amplitude remains generally unchanged (0 % in the MMM), although most models show either increase or decrease. Altogether, these features suggest that PDO might have been a more relevant mode of climate variability in the MP than in the PI because ENSO decreased its importance.

The relationship between ENSO and PDO was analysed through quantifying correlation coefficients. We find that the linear relation between ENSO and PDO is reduced in the MP (by 18 % in the MMM) in 4 out of 7 PlioMIP2 models and that ENSO leads PDO by 4–8 months. Correlation coefficients are reduced, even though ENSO variability is much more reduced. Furthermore, slight differences in the lagged correlation suggest that the physical mechanism of the ENSO–PDO relationship is similar in the MP and PI. In consequence, we suggest that the physical mechanism that explains a similar PDO variability regardless of ENSO suppression might not be related to ENSO. In addition, using sensitivity simulations, we find that changes in the MP PDO are largely driven by the MP boundary conditions other than elevated CO_2 (e.g. closed seaways and reduced ice sheets). A large part of the PDO change (~70 %) in the MP might be related to changes in the North Pacific atmospheric variability, which is unchanged in the MP compared to the PI, as Oldeman et al. (2024) found for the North Pacific variability itself. Nevertheless, we cannot state whether the teleconnection between the North Pacific atmosphere and PDO changes. Future work exploring this physical link is necessary. Meanwhile, we hypothesize that other factors, such as the Arctic sea-ice variability might have an important impact on PDO variability that should also be explored.

Data and code availability

Data access enquiries could be initially directed to Julia Tindall (j.c.tindall@leeds.ac.uk). Datasets from IPSL-CM6A-LR were downloaded from the CMIP6 repository (https://esgf-node.llnl.gov/search/cmip6/). Analysis codes are publicly available as jupyter notebooks on Zenodo (https://doi.org/10.5281/zenodo.15653026).

CRediT authorship contribution statement

Katya V. Canal-Solis: Writing – original draft, Visualization, Formal analysis, Conceptualization. **Julia C. Tindall:** Writing – review & editing, Supervision, Software, Conceptualization. **Arthur M. Oldeman:** Writing – review & editing, Conceptualization. **Alan M. Haywood:** Writing – review & editing, Conceptualization. **Ayako Abe-Ouchi:** Writing – review & editing, Software. **Michiel L.J. Baatsen:** Writing – review & editing, Software. **Wing-Le Chan:** Writing – review & editing, Software. **Ran Feng:** Writing – review & editing, Software. **Stephen J. Hunter:** Writing – review & editing, Software. **Xiangyu Li:** Writing – review & editing, Software. **Christian Stepanek:** Writing – review & editing, Software. **Zhongshi Zhang:** Writing – review & editing, Software.

Financial support

This research has been supported by the Past Earth Network (EPSRC grant no. EP/M008.363/1).

Declaration of competing interest

Alan M. Haywood is editor-in-chief of Global and Planetary Change but the review will be independent.

The authors declare that they have no known competing financial interests or personal relationships that could have appeared to influence the work reported in this paper.

Acknowledgements

Julia C. Tindall was supported through the Centre for Environmental Modelling and Computation (CEMAC), University of Leeds.

Arthur M. Oldeman and Michiel L. J. Baatsen acknowledge support by the programme of the Netherlands Earth System Science Centre (NESSC), financially supported by the Ministry of Education, Culture and Science (OCW grant no. 024.002.001).

Ayako Abe-Ouchi and Wing-Le Chan acknowledge financial support from Grants-in-Aid for Scientific Research (KAKEN), grant numbers 17H06104, 17H06323 and 24H02346.

Ran Feng acknowledges U.S. NSF-2103055 for supporting the development of the CESM1.2 MP simulation.

Christian Stepanek acknowledges institutional funding from the Alfred Wegener Institute (AWI) through the research program PACES-II of the Helmholtz Association and from the Helmholtz Climate Initiative REKLIM.

Xiangyu Li acknowledges funding from National Natural Science Foundation of China (42005042 and 42275047).

Zhongshi Zhang acknowledges financial support from the National Natural Science Foundation of China (42125502).

The authors would also like to thank Trude Storelvmo and the two anonymous reviewers for their valuable feedback, which helped improve the manuscript.

Appendix A. Supplementary data

Supplementary data to this article can be found online at https://doi.org/10.1016/j.gloplacha.2025.104932.

References

Alexander, M.A., Bladé, I., Newman, M., Lanzante, J.R., Lau, N.-C., Scott, J.D., 2002. The atmospheric bridge: the influence of ENSO teleconnections on air–sea interaction over the global oceans. J. Climate 15, 2205–2231. https://doi.org/10.1175/1520-0442(2002)015<2205:TABTIO>2.0.CO;2.

Baatsen, M.L.J., Von Der Heydt, A.S., Kliphuis, M.A., Oldeman, A.M., Weiffenbach, J.E., 2022. Warm mid-Pliocene conditions without high climate sensitivity: the CCSM4-Utrecht (CESM 1.0.5) contribution to the PlioMIP2. Clim. Past 18, 657–679. https://doi.org/10.5194/cp-18-657-2022.

Bonham, S.G., Haywood, A.M., Lunt, D.J., Collins, M., Salzmann, U., 2009. El Niño–Southern Oscillation, Pliocene climate and equifinality. Phil. Trans. R. Soc. A 367, 127–156. https://doi.org/10.1098/rsta.2008.0212.

Brierley, C.M., 2015. Interannual climate variability seen in the Pliocene Model Intercomparison Project. Clim. Past 11, 605–618. https://doi.org/10.5194/cp-11-605-2015.

Burke, K.D., Williams, J.W., Chandler, M.A., Haywood, A.M., Lunt, D.J., Otto-Bliesner, B.L., 2018. Pliocene and Eocene provide best analogs for near-future climates. Proc. Natl. Acad. Sci. U. S. A. 115, 13288–13293. https://doi.org/10.1073/pnas.1809600115.

Burton, L., Oldeman, A.M., Haywood, A.M., Tindall, J.C., Dolan, A., Hill, D.J., Von Der Heydt, A., Baatsen, M.L.J., 2024. An Assessment of the Pliocene as an Analogue for Our Warmer Future. https://doi.org/10.2139/ssrn.4924028.

Cai, W., Borlace, S., Lengaigne, M., Van Rensch, P., Collins, M., Vecchi, G., Timmermann, A., Santoso, A., McPhaden, M.J., Wu, L., England, M.H., Wang, G., Guilyardi, E., Jin, F.-F., 2014. Increasing frequency of extreme El Niño events due to greenhouse warming. Nature Clim Change 4, 111–116. https://doi.org/10.1038/nclimate2100.

Carvalho, K.S., Wang, S., 2020. Sea surface temperature variability in the Arctic Ocean and its marginal seas in a changing climate: patterns and mechanisms. Global Planet. Change 193, 103265. https://doi.org/10.1016/j.gloplacha.2020.103265.

Chan, W.-L., Abe-Ouchi, A., 2020. Pliocene Model Intercomparison Project (PlioMIP2) simulations using the Model for Interdisciplinary Research on Climate (MIROC4m). Clim. Past 16, 1523–1545. https://doi.org/10.5194/cp-16-1523-2020.

Chandan, D., Peltier, W.R., 2017. Regional and global climate for the mid-Pliocene using the University of Toronto version of CCSM4 and PlioMIP2 boundary conditions. Clim. Past 13, 919–942. https://doi.org/10.5194/cp-13-919-2017.

Colas, F., McWilliams, J.C., Capet, X., Kurian, J., 2012. Heat balance and eddies in the Peru-Chile current system. Climate Dynam. 39, 509–529. https://doi.org/10.1007/s00382-011-1170-6.

De Nooijer, W., Zhang, Q., Li, Q., Zhang, Q., Li, X., Zhang, Z., Guo, C., Nisancioglu, K.H., Haywood, A.M., Tindall, J.C., Hunter, S.J., Dowsett, H.J., Stepanek, C., Lohmann, G., Otto-Bliesner, B.L., Feng, R., Sohl, L.E., Chandler, M.A., Tan, N., Contoux, C., Ramstein, G., Baatsen, M.L.J., Von Der Heydt, A.S., Chandan, D., Peltier, W.R., Abe-Ouchi, A., Chan, W.-L., Kamae, Y., Brierley, C.M., 2020. Evaluation of Arctic warming in mid-Pliocene climate simulations. Clim. Past 16, 2325–2341. https://doi.org/10.5194/cp-16-2325-2020.

Di Lorenzo, E., Combes, V., Keister, J., Strub, P.T., Thomas, A., Franks, P., Ohman, M., Furtado, J., Bracco, A., Bograd, S., Peterson, W., Schwing, F., Chiba, S., Taguchi, B., Hormazabal, S., Parada, C., 2013. Synthesis of Pacific Ocean climate and ecosystem dynamics. oceanog 26, 68–81. https://doi.org/10.5670/oceanog.2013.76.

Dommenget, D., Latif, M., 2002. A cautionary note on the interpretation of EOFs. J. Climate 15, 216–225. https://doi.org/10.1175/1520-0442(2002)015<0216:ACNOTI>2.0.CO;2.

Dowsett, H., Dolan, A., Rowley, D., Moucha, R., Forte, A.M., Mitrovica, J.X., Pound, M., Salzmann, U., Robinson, M., Chandler, M., Foley, K., Haywood, A., 2016. The PRISM4 (mid-Piacenzian) paleoenvironmental reconstruction. Clim. Past 12, 1519–1538. https://doi.org/10.5194/cp-12-1519-2016.

Fedorov, A.V., Dekens, P.S., McCarthy, M., Ravelo, A.C., deMenocal, P.B., Barreiro, M., Pacanowski, R.C., Philander, S.G., 2006. The Pliocene Paradox (Mechanisms for a Permanent El Niño). Science 312, 1485–1489. https://doi.org/10.1126/science.1122666.

Feng, R., Otto-Bliesner, B.L., Brady, E.C., Rosenbloom, N., 2020. Increased climate response and earth system sensitivity from CCSM4 to CESM2 in Mid-Pliocene simulations. J Adv Model Earth Syst 12, e2019MS002033. https://doi.org/10.1029/2019MS002033.

Foley, K.M., Dowsett, H.J., 2019. Community Sourced Mid-Piacenzian Sea Surface Temperature (SST) Data. https://doi.org/10.5066/P9YP3DTV.

Geng, T., Yang, Y., Wu, L., 2019. On the mechanisms of Pacific decadal oscillation modulation in a warming climate. J. Climate 32, 1443–1459. https://doi.org/10.1175/JCLI-D-18-0337.1.

Geng, T., Jia, F., Cai, W., Wu, L., Gan, B., Jing, Z., Li, S., McPhaden, M.J., 2023. Increased occurrences of consecutive La Niña events under global warming. Nature 619, 774–781. https://doi.org/10.1038/s41586-023-06236-9.

Ghil, M., Allen, M.R., Dettinger, M.D., Ide, K., Kondrashov, D., Mann, M.E., Robertson, A.W., Saunders, A., Tian, Y., Varadi, F., Yiou, P., 2002. Advanced spectral methods for climatic time series. Rev. Geophys. 40. https://doi.org/10.1029/2000RG000092.

Glantz, M.H., Ramirez, I.J., 2020. Reviewing the Oceanic Niño Index (ONI) to enhance societal readiness for El Niño's impacts. Int. J. Disaster Risk Sci. 11, 394–403. https://doi.org/10.1007/s13753-020-00275-w.

Han, Z., Zhang, Q., Li, Q., Feng, R., Haywood, A.M., Tindall, J.C., Hunter, S.J., Otto-Bliesner, B.L., Brady, E.C., Rosenbloom, N., Zhang, Z., Li, X., Guo, C., Nisancioglu, K.H., Stepanek, C., Lohmann, G., Sohl, L.E., Chandler, M.A., Tan, N., Ramstein, G., Baatsen, M.L.J., Von Der Heydt, A.S., Chandan, D., Peltier, W.R., Williams, C.J.R., Lunt, D.J., Cheng, J., Wen, Q., Burls, N.J., 2021. Evaluating the large-scale hydrological cycle response within the Pliocene Model Intercomparison Project Phase 2 (PlioMIP2) ensemble. Clim. Past 17, 2537–2558. https://doi.org/10.5194/cp-17-2537-2021.

Hare, S.R., Mantua, N.J., 2000. Empirical evidence for North Pacific regime shifts in 1977 and 1989. Prog. Oceanogr. 47, 103–145. https://doi.org/10.1016/S0079-6611(00)00033-1.

Haywood, A.M., Valdes, P.J., Peck, V.L., 2007. A permanent El Niño–like state during the Pliocene? Paleoceanography 22, 2006PA001323. https://doi.org/10.1029/2006PA001323.

Haywood, A.M., Dowsett, H.J., Otto-Bliesner, B., Chandler, M.A., Dolan, A.M., Hill, D.J., Lunt, D.J., Robinson, M.M., Rosenbloom, N., Salzmann, U., Sohl, L.E., 2010. Pliocene Model Intercomparison Project (PlioMIP): experimental design and boundary conditions (Experiment 1). Geosci. Model Dev. 3, 227–242. https://doi.org/10.5194/gmd-3-227-2010.

Haywood, A.M., Dowsett, H.J., Dolan, A.M., Rowley, D., Abe-Ouchi, A., Otto-Bliesner, B., Chandler, M.A., Hunter, S.J., Lunt, D.J., Pound, M., Salzmann, U., 2016. The Pliocene Model Intercomparison Project (PlioMIP) Phase 2: scientific objectives and experimental design. Clim. Past 12, 663–675. https://doi.org/10.5194/cp-12-663-2016.

Haywood, A.M., Tindall, J.C., Dowsett, H.J., Dolan, A.M., Foley, K.M., Hunter, S.J., Hill, D.J., Chan, W.-L., Abe-Ouchi, A., Stepanek, C., Lohmann, G., Chandan, D., Peltier, W.R., Tan, N., Contoux, C., Ramstein, G., Li, X., Zhang, Z., Guo, C., Nisancioglu, K.H., Zhang, Q., Li, Q., Kamae, Y., Chandler, M.A., Sohl, L.E., Otto-Bliesner, B.L., Feng, R., Brady, E.C., Von Der Heydt, A.S., Baatsen, M.L.J., Lunt, D.J., 2020. The Pliocene Model Intercomparison Project Phase 2: large-scale climate features and climate sensitivity. Clim. Past 16, 2095–2123. https://doi.org/10.5194/cp-16-2095-2020.

Haywood, A.M., Tindall, J.C., Burton, L.E., Chandler, M.A., Dolan, A.M., Dowsett, H.J., Feng, R., Fletcher, T.L., Foley, K.M., Hill, D.J., Hunter, S.J., Otto-Bliesner, B.L., Lunt, D.J., Robinson, M.M., Salzmann, U., 2024. Pliocene Model Intercomparison Project Phase 3 (PlioMIP3) – science plan and experimental design. Global Planet. Change 232, 104316. https://doi.org/10.1016/j.gloplacha.2023.104316.

Hsu, P.-C., Ho, C.-R., Liang, S.-J., Kuo, N.-J., 2013. Impacts of two types of El Niño and La Niña events on typhoon activity. Adv. Meteorol. 1–8, 2013. https://doi.org/10.1155/2013/632470.

Hu, A., Meehl, G.A., Han, W., Otto-Bliestner, B., Abe-Ouchi, A., Rosenbloom, N., 2015. Effects of the Bering Strait closure on AMOC and global climate under different background climates. Prog. Oceanogr. 132, 174–196. https://doi.org/10.1016/j.pocean.2014.02.004.

Huang, B., Thorne, P.W., Banzon, V.F., Boyer, T., Chepurin, G., Lawrimore, J.H., Menne, M.J., Smith, T.M., Vose, R.S., Zhang, H.-M., 2017. Extended Reconstructed Sea Surface Temperature, Version 5 (ERSSTv5): upgrades, validations, and intercomparisons. Journal of Climate 30, 8179–8205. https://doi.org/10.1175/JCLI-D-16-0836.1.

Hunter, S.J., Haywood, A.M., Dolan, A.M., Tindall, J.C., 2019. The HadCM3 contribution to PlioMIP phase 2. Clim. Past 15, 1691–1713. https://doi.org/10.5194/cp-15-1691-2019.

Kim, S.T., Cai, W., Jin, F.-F., Santoso, A., Wu, L., Guilyardi, E., An, S.-I., 2014. Response of El Niño sea surface temperature variability to greenhouse warming. Nature Clim Change 4, 786–790. https://doi.org/10.1038/nclimate2326.

Kim, H., Yeh, S.-W., An, S.-I., Song, S.-Y., 2020. Changes in the role of Pacific decadal oscillation on sea ice extent variability across the mid-1990s. Sci. Rep. 10, 17564. https://doi.org/10.1038/s41598-020-74260-0.

King, A.D., Lane, T.P., Henley, B.J., Brown, J.R., 2020. Global and regional impacts differ between transient and equilibrium warmer worlds. Nat. Clim. Chang. 10, 42–47. https://doi.org/10.1038/s41558-019-0658-7.

Kwon, M., Yeh, S., Park, Y., Lee, Y., 2013. Changes in the linear relationship of ENSO–PDO under the global warming. Int. J. Climatol. 33, 1121–1128. https://doi.org/10.1002/joc.3497.

Lee, J.-Y., Marotzke, J., Bala, G., Cao, L., Corti, S., Dunne, J.P., Engelbrecht, F., Fischer, E., Fyfe, J.C., Jones, C., Maycock, A., Mutemi, J., Ndiaye, O., Panickal, S., Zhou, T., 2023. Future global climate: scenario-based projections and near-term information. In: Climate Change 2021: The Physical Science Basis. Contribution of Working Group I to the Sixth Assessment Report of the Intergovernmental Panel on Climate Change. Cambridge University Press.

Li, G., Xie, S., 2012. Origins of tropical-wide SST biases in CMIP multi-model ensembles. Geophys. Res. Lett. 39, 2012GL053777. https://doi.org/10.1029/2012GL053777.

Li, X., Guo, C., Zhang, Z., Otterå, O.H., Zhang, R., 2020. PlioMIP2 simulations with NorESM-L and NorESM1-F. Clim. Past 16, 183–197. https://doi.org/10.5194/cp-16-183-2020.

Li, S., Wu, L., Yang, Y., Geng, T., Cai, W., Gan, B., Chen, Z., Jing, Z., Wang, G., Ma, X., 2020. The Pacific Decadal Oscillation less predictable under greenhouse warming. Nat. Clim. Chang. 10, 30–34. https://doi.org/10.1038/s41558-019-0663-x.

Liguori, G., Lorenzo, E.D., 2018. Meridional modes and increasing Pacific decadal variability under anthropogenic forcing. Geophys. Res. Lett. 45, 983–991. https://doi.org/10.1002/2017GL076548.

Lurton, T., Balkanski, Y., Bastrikov, V., Bekki, S., Bopp, L., Braconnot, P., Brockmann, P., Cadule, P., Contoux, C., Cozic, A., Cugnet, D., Dufresne, J., Éthé, C., Foujols, M., Ghattas, J., Hauglustaine, D., Hu, R., Kageyama, M., Khodri, M., Lebas, N., Levavasseur, G., Marchand, M., Ottlé, C., Peylin, P., Sima, A., Szopa, S., Thiéblemont, R., Vuichard, N., Boucher, O., 2020. Implementation of the CMIP6 forcing data in the IPSL-CM6A-LR Model. J Adv Model Earth Syst 12, e2019MS001940. https://doi.org/10.1029/2019MS001940.

Ma, C.-C., Mechoso, C.R., Robertson, A.W., Arakawa, A., 1996. Peruvian stratus clouds and the tropical pacific circulation: a coupled ocean-atmosphere GCM study. J. Climate 9, 1635–1645. https://doi.org/10.1175/1520-0442(1996)009<1635:PSCATT>2.0.CO;2.

Mantua, N.J., Hare, S.R., 2002. The Pacific decadal oscillation. J. Oceanogr. 58, 35–44. https://doi.org/10.1023/A:1015820616384.

Mantua, N.J., Hare, S.R., Zhang, Y., Wallace, J.M., Francis, R.C., 1997. A Pacific interdecadal climate oscillation with impacts on salmon production. Bull. Amer. Meteor. Soc. 78, 1069–1079. https://doi.org/10.1175/1520-0477(1997)078<1069:APICOW>2.0.CO;2.

McClymont, E.L., Ford, H.L., Ho, S.L., Tindall, J.C., Haywood, A.M., Alonso-Garcia, M., Bailey, I., Berke, M.A., Littler, K., Patterson, M.O., Petrick, B., Peterse, F., Ravelo, A. C., Risebrobakken, B., De Schepper, S., Swann, G.E.A., Thirumalai, K., Tierney, J.E., Van Der Weijst, C., White, S., Abe-Ouchi, A., Baatsen, M.L.J., Brady, E.C., Chan, W.-L., Chandan, D., Feng, R., Guo, C., Von Der Heydt, A.S., Hunter, S., Li, X., Lohmann, G., Nisancioglu, K.H., Otto-Bliesner, B.L., Peltier, W.R., Stepanek, C., Zhang, Z., 2020. Lessons from a high-CO₂ world: an ocean view from ~3 million years ago. Clim. Past 16, 1599–1615. https://doi.org/10.5194/cp-16-1599-2020.

McPhaden, M.J., Zebiak, S.E., Glantz, M.H., 2006. ENSO as an Integrating Concept in Earth Science. Science 314, 1740–1745. https://doi.org/10.1126/science.1132588.

Molnar, P., Cane, M.A., 2002. El Niño's tropical climate and teleconnections as a blueprint for pre-Ice Age climates. Paleoceanography 17. https://doi.org/10.1029/2001PA000663.

Newman, M., 2007. Interannual to decadal predictability of tropical and north Pacific sea surface temperatures. J. Climate 20, 2333–2356. https://doi.org/10.1175/JCLI4165.1.

Newman, M., Alexander, M.A., Ault, T.R., Cobb, K.M., Deser, C., Di Lorenzo, E., Mantua, N.J., Miller, A.J., Minobe, S., Nakamura, H., Schneider, N., Vimont, D.J., Phillips, A.S., Scott, J.D., Smith, C.A., 2016. The Pacific decadal oscillation, revisited. Journal of Climate 29, 4399–4427. https://doi.org/10.1175/JCLI-D-15-0508.1.

Nidheesh, A.G., Lengaigne, M., Vialard, J., Izumo, T., Unnikrishnan, A.S., Cassou, C., 2017. Influence of ENSO on the Pacific decadal oscillation in CMIP models. Climate Dynam. 49, 3309–3326. https://doi.org/10.1007/s00382-016-3514-8.

Oldeman, A., 2021. arthuroldeman/pliomip2-enso: v1.0. https://doi.org/10.5281/ZENODO.5718483.

Oldeman, A.M., Baatsen, M.L.J., Von Der Heydt, A.S., Dijkstra, H.A., Tindall, J.C., Abe-Ouchi, A., Booth, A.R., Brady, E.C., Chan, W.-L., Chandan, D., Chandler, M.A., Contoux, C., Feng, R., Guo, C., Haywood, A.M., Hunter, S.J., Kamae, Y., Li, Q., Li, X., Lohmann, G., Lunt, D.J., Nisancioglu, K.H., Otto-Bliesner, B.L., Peltier, W.R., Pontes, G.M., Ramstein, G., Sohl, L.E., Stepanek, C., Tan, N., Zhang, Q., Zhang, Z., Wainer, I., Williams, C.J.R., 2021. Reduced El Niño variability in the mid-Pliocene according to the PlioMIP2 ensemble. Clim. Past 17, 2427–2450. https://doi.org/10.5194/cp-17-2427-2021.

Oldeman, A.M., Baatsen, M.L.J., Von Der Heydt, A.S., Selten, F.M., Dijkstra, H.A., 2024. Similar North Pacific variability despite suppressed El Niño variability in the warm mid-Pliocene climate. Earth Syst. Dynam. 15, 1037–1054. https://doi.org/10.5194/esd-15-1037-2024.

Otto-Bliesner, B.L., Jahn, A., Feng, R., Brady, E.C., Hu, A., Löfverström, M., 2017a. Amplified North Atlantic warming in the late Pliocene by changes in Arctic gateways. Geophys. Res. Lett. 44, 957–964. https://doi.org/10.1002/2016GL071805.

Otto-Bliesner, B.L., Braconnot, P., Harrison, S.P., Lunt, D.J., Abe-Ouchi, A., Albani, S., Bartlein, P.J., Capron, E., Carlson, A.E., Dutton, A., Fischer, H., Goelzer, H., Govin, A., Haywood, A., Joos, F., LeGrande, A.N., Lipscomb, W.H., Lohmann, G., Mahowald, N., Nehrbass-Ahles, C., Pausata, F.S.R., Peterschmitt, J.-Y., Phipps, S.J., Renssen, H., Zhang, Q., 2017b. The PMIP4 contribution to CMIP6 – part 2: two interglacials, scientific objective and experimental design for Holocene and Last Interglacial simulations. Geosci. Model Dev. 10, 3979–4003. https://doi.org/10.5194/gmd-10-3979-2017.

PALAEOSENS Project Members, 2012. Making sense of palaeoclimate sensitivity. Nature 491, 683–691. https://doi.org/10.1038/nature11574.

Pontes, G.M., Taschetto, A.S., Sen Gupta, A., Santoso, A., Wainer, I., Haywood, A.M., Chan, W.-L., Abe-Ouchi, A., Stepanek, C., Lohmann, G., Hunter, S.J., Tindall, J.C., Chandler, M.A., Sohl, L.E., Peltier, W.R., Chandan, D., Kamae, Y., Nisancioglu, K.H., Zhang, Z., Contoux, C., Tan, N., Zhang, Q., Otto-Bliesner, B.L., Brady, E.C., Feng, R., Von Der Heydt, A.S., Baatsen, M.L.J., Oldeman, A.M., 2022. Mid-Pliocene El Niño/Southern Oscillation suppressed by Pacific intertropical convergence zone shift. Nat. Geosci. 15, 726–734. https://doi.org/10.1038/s41561-022-00999-y.

Power, S., Delage, F., Chung, C., Kociuba, G., Keay, K., 2013. Robust twenty-first-century projections of El Niño and related precipitation variability. Nature 502, 541–545. https://doi.org/10.1038/nature12580.

Ravelo, A.C., Simonne Dekens, P., McCarthy, M., 2006. Evidence for El Niño–like conditions during the Pliocene. GSA Today 16, 4. https://doi.org/10.1130/1052-5173(2006)016<4:EFENLC>2.0.CO;2.

Ren, X., Lunt, D.J., Hendy, E., Von Der Heydt, A., Abe-Ouchi, A., Otto-Bliesner, B., Williams, C.J.R., Stepanek, C., Guo, C., Chandan, D., Lohmann, G., Tindall, J.C., Sohl, L.E., Chandler, M.A., Kageyama, M., Baatsen, M.L.J., Tan, N., Zhang, Q., Feng, R., Hunter, S., Chan, W.-L., Peltier, W.R., Li, X., Kamae, Y., Zhang, Z., Haywood, A.M., 2023. The hydrological cycle and ocean circulation of the Maritime Continent in the Pliocene: results from PlioMIP2. Clim. Past 19, 2053–2077. https://doi.org/10.5194/cp-19-2053-2023.

Salzmann, U., Haywood, A.M., Lunt, D.J., Valdes, P.J., Hill, D.J., 2008. A new global biome reconstruction and data-model comparison for the Middle Pliocene. Glob. Ecol. Biogeogr. 17, 432–447. https://doi.org/10.1111/j.1466-8238.2008.00381.x.

Samakinwa, E., Stepanek, C., Lohmann, G., 2020. Sensitivity of mid-Pliocene climate to changes in orbital forcing and PlioMIP's boundary conditions. Clim. Past 16, 1643–1665. https://doi.org/10.5194/cp-16-1643-2020.

Scroxton, N., Bonham, S.G., Rickaby, R.E.M., Lawrence, S.H.F., Hermoso, M., Haywood, A.M., 2011. Persistent El Niño–Southern Oscillation variation during the Pliocene Epoch. Paleoceanography 26, 2010PA002097. https://doi.org/10.1029/2010PA002097.

Seki, O., Schmidt, D.N., Schouten, S., Hopmans, E.C., Sinninghe Damsté, J.S., Pancost, R. D., 2012. Paleoceanographic changes in the Eastern Equatorial Pacific over the last 10 Myr. Paleoceanography 27, 2011PA002158. https://doi.org/10.1029/2011PA002158.

Sherwood, S.C., Webb, M.J., Annan, J.D., Armour, K.C., Forster, P.M., Hargreaves, J.C., Hegerl, G., Klein, S.A., Marvel, K.D., Rohling, E.J., Watanabe, M., Andrews, T., Braconnot, P., Bretherton, C.S., Foster, G.L., Hausfather, Z., Von Der Heydt, A.S., Knutti, R., Mauritsen, T., Norris, J.R., Proistosescu, C., Rugenstein, M., Schmidt, G. A., Tokarska, K.B., Zelinka, M.D., 2020. An assessment of Earth's climate sensitivity using multiple lines of evidence. Rev. Geophys. 58, e2019RG000678. https://doi.org/10.1029/2019RG000678.

Simon, A., Gastineau, G., Frankignoul, C., Lapin, V., Ortega, P., 2022. Pacific Decadal Oscillation modulates the Arctic sea-ice loss influence on the midlatitude atmospheric circulation in winter. Weather Clim. Dynam. 3, 845–861. https://doi.org/10.5194/wcd-3-845-2022.

Stepanek, C., Samakinwa, E., Knorr, G., Lohmann, G., 2020. Contribution of the coupled atmosphere–ocean–sea ice–vegetation model COSMOS to the PlioMIP2. Clim. Past 16, 2275–2323. https://doi.org/10.5194/cp-16-2275-2020.

Tindall, J.C., Haywood, A.M., Howell, F.W., 2016. Accounting for centennial-scale variability when detecting changes in ENSO: a study of the Pliocene: PLIOCENE ENSO. Paleoceanography 31, 1330–1349. https://doi.org/10.1002/2016PA002951.

Tindall, J.C., Haywood, A.M., Salzmann, U., Dolan, A.M., Fletcher, T., 2022. The warm winter paradox in the Pliocene northern high latitudes. Clim. Past 18, 1385–1405. https://doi.org/10.5194/cp-18-1385-2022.

Trenberth, K.E., Fasullo, J.T., 2013. An apparent hiatus in global warming? Earth's Future 1, 19–32. https://doi.org/10.1002/2013EF000165.

Vaideanu, P., Stepanek, C., Dima, M., Schrepfer, J., Matos, F., Ionita, M., Lohmann, G., 2023. Large-scale sea ice–Surface temperature variability linked to Atlantic meridional overturning circulation. PloS One 18, e0290437. https://doi.org/10.1371/journal.pone.0290437.

Verdon, D.C., Franks, S.W., 2006. Long-term behaviour of ENSO: Interactions with the PDO over the past 400 years inferred from paleoclimate records. Geophys. Res. Lett. 33, 2005GL025052. https://doi.org/10.1029/2005GL025052.

von der Heydt, A.S., Nnafie, A., Dijkstra, H.A., 2011. Cold tongue/warm pool and ENSO dynamics in the Pliocene. Clim. Past 7, 903–915. https://doi.org/10.5194/cp-7-903-2011.

Wang, C., 2019. Three-ocean interactions and climate variability: a review and perspective. Climate Dynam. 53, 5119–5136. https://doi.org/10.1007/s00382-019-04930-x.

Wang, G., Hendon, H.H., 2007. Sensitivity of Australian rainfall to inter–El Niño variations. J. Climate 20, 4211–4226. https://doi.org/10.1175/JCLI4228.1.

Wara, M.W., Ravelo, A.C., Delaney, M.L., 2005. Permanent El Niño-like conditions during the Pliocene warm period. Science 309, 758–761. https://doi.org/10.1126/science.1112596.

Watanabe, T., Suzuki, A., Minobe, S., Kawashima, T., Kameo, K., Minoshima, K., Aguilar, Y.M., Wani, R., Kawahata, H., Sowa, K., Nagai, T., Kase, T., 2011. Permanent El Niño during the Pliocene warm period not supported by coral evidence. Nature 471, 209–211. https://doi.org/10.1038/nature09777.

Weiffenbach, J.E., Baatsen, M.L.J., Dijkstra, H.A., Von Der Heydt, A.S., Abe-Ouchi, A., Brady, E.C., Chan, W.-L., Chandan, D., Chandler, M.A., Contoux, C., Feng, R., Guo, C., Han, Z., Haywood, A.M., Li, Q., Li, X., Lohmann, G., Lunt, D.J., Nisancioglu, K.H., Otto-Bliesner, B.L., Peltier, W.R., Ramstein, G., Sohl, L.E., Stepanek, C., Tan, N., Tindall, J.C., Williams, C.J.R., Zhang, Q., Zhang, Z., 2023. Unraveling the mechanisms and implications of a stronger mid-Pliocene Atlantic Meridional Overturning Circulation (AMOC) in PlioMIP2. Clim. Past 19, 61–85. https://doi.org/10.5194/cp-19-61-2023.

White, S.M., Ravelo, A.C., 2020. Dampened El Niño in the early Pliocene warm period. Geophys. Res. Lett. 47, e2019GL085504. https://doi.org/10.1029/2019GL085504.

Wu, S., Liu, Z.-Y., 2020. Decadal variability in the North Pacific and North Atlantic under global warming: the weakening response and its mechanism. J. Climate 33, 9181–9193. https://doi.org/10.1175/JCLI-D-19-1012.1.

Yan, X., Boyer, T., Trenberth, K., Karl, T.R., Xie, S., Nieves, V., Tung, K., Roemmich, D., 2016. The global warming hiatus: slowdown or redistribution? Earth's Future 4, 472–482. https://doi.org/10.1002/2016EF000417.

Yang, X.-Y., Wang, G., Keenlyside, N., 2020. The Arctic sea ice extent change connected to Pacific decadal variability. Cryosphere 14, 693–708. https://doi.org/10.5194/tc-14-693-2020.

Zhang, Z., Qing, Y., Jing-Zhi, S., Yong-Qi, G., 2012. Has the problem of a permanent El Niño been resolved for the Mid-Pliocene? Atmospheric and Oceanic Science Letters 5, 445–448. https://doi.org/10.1080/16742834.2012.11447035.